Title
Bispecific Antibody Targeted Stem Cell Therapy for Myocardial Repair

Author
Gu, Yiping

Publication Date
2008

Peer reviewed|Thesis/dissertation

Bispecific Antibody Targeted Stem Cell Therapy for Myocardial Repair

by

Yiping Gu

DISSERTATION

Submitted in partial satisfaction of the requirements for the degree of

DOCTOR OF PHILOSOPHY

in

Bioengineering

in the

GRADUATE DIVISION

of the

UNIVERSITY OF CALIFORNIA, SAN FRANCISCO

AND

UNIVERSITY OF CALIFORNIA, BERKELEY

Abstract

Bispecific Antibody Targeted Stem Cell Therapy for Myocardial Repair

by

Yiping Gu

Doctor of Philosophy in the Graduate Division of the
University of California, San Francisco
and
University of California, Berkeley

Cardiac cell therapy for myocardial infarction has been extensively studied due to its regenerative potential. However, the success of cardiac cell therapy is greatly limited by delivery efficiency, cell fate after delivery, and possible proarrhythmia associated with some cell types. To successfully improve efficiency of cardiac cell therapy, we herein proposed a new bispecific antibody (BiAb) targeting technology to efficiently deliver therapeutical cells to myocardial injury by chemically linking monoclonal antibody specifics to myocardial injury and another monoclonal antibody binding to the therapeutical cells. To reach this goal, in this work, we first optimized the method to arm BiAb to human hematopoietic stem cells (hHSCs) and consequently verified that the BiAb armed hHSCs could be successfully and efficiently delivered to injured myocardium. By comparing and contrasting the BiAb targeting method with more conventional systematical administration and direct injection into damaged myocardium;, we investigated the beneficial effect of hHSCs in improving/preserving cardiac function and reducing the size of infarction and explored the angiogenic mechanism of hHSCs in

myocardial infarction. We also studied whether or not hHSCs are proarrhythmic by comparing the ventricular tachycardia inducibility, effective refractory period and conduction velocity between treatment and a control group and a new analytic method of electrophysiological data was proposed and compared with traditional approaches based on time series analysis.

Overall results in this work demonstrated that BiAb targeting is significantly better than systematical administration and comparable, if not better, to direction injection in terms of preserving cardiac function, reducing myocardial infarction size, and promoting angiogenesis in myocardial infarction. Human HSCs are not proarrhythmic and hHSCs targeted by BiAb showed improved electrophysiological properties than control group. Therefore we concluded that BiAb targeting is an effective and efficiently delivery method and it further leads the therapeutical cells to a more favorable milieu to help the cell survival; hHSCs preserved cardiac function with the aid of BiAb through angiogenesis.

Approved

_____

Randall Lee, PhD MD

Dissertation Chairperson

Table of Contents

Chapter 1: Introduction……1
1.1 Coronary heart disease, myocardial infarction and cardiac arrhythmia ……...1
1.2 Pathology and physiology ……2
1.3 Current Treatments……3
1.4 Bioengineering approaches in cardiac research……4
1.4.1 Cell therapy……4
1.4.2 Antibody targeting technology……...7
1.4.3 Biomaterials ……8
Chapter 2: General Methods……9
2.1 Introduction……9
2.2 Rat acute myocardial infarct model and cell administration……9
2.3 Echocardiography……10
2.4 Tissue collection and fresh frozen sectioning ……11
2.5 Histochemical assessment ……12
Chapter 3: Bispecific Antibody ……13
3.1 Introduction ……13
3.2 Methods ……14
3.2.1 Conjugation of bispecific antibody……14
3.2.2 Flow Cytometry ……15
3.3 Results ……15
3.3.1 Conjugation of CD45 x MLC BiAb ……15
3.3.2 CD45 x MLC binding efficiency curve ……16
3.4 Discussion ……18
Chapter 4: Detection of BiAb homed stem cells with MRI ……20
4.1 Introduction ……20
4.2 Method ……21
4.2.1 Cell labeling ……21
4.2.2 Arming of human CD34+ cells ……21
4.2.3 Prussian blue staining of iron particles……22
4.3 results……22
4.3.1 Iron-labeled cells are detectable under MRI……22
4.3.2 SPIO-labeled homed cells were correlated in histology and MRI....24
4.4 Discussion ……25
Chapter 5: BiAb armed HSCs preserves cardiac function ……27
5.1 Introduction ……27
5.2 Methods ……29
5.2.1 Rat acute MI model ……29
5.2.2 Arming of human hematopoietic cells ……29
5.2.3 Administration of CD34+ cells ……29
5.2.4 Echocardiography ……29
5.2.5 Immunofluorescence staining ……30
A. Staining of vasculatures …….. 30
B. Staining of myocytes ……30
5.2.6 Statistics ……31
5.3 Results ……31

5.3.1 CD45 x MLC BiAb armed HSCs prevented negative remodeling...31
5.3.2 More HSCs in MI border zone in armed group and coexpress human marker and myocyte specific antigen with gap junction proteins ……32
5.3.3 HSCs may transdifferentiate to smooth muscle cells…… 34
5.4 Discussion ……35
Chapter 6:
BiAb-homed HSCs preserves cardiac function as efficient as direct injection ……37
6.1 Introduction ……37
6.2 Methods ……..39
6.2.1 Rat acute MI model ……..39
6.2.2 Arming of human CD34+ cells ……39
6.2.3 Administration of CD34+ cells ……39
6.2.4 Echocardiography ……39
6.2.5 Histology ……39
6.2.6 Statistics ……...40
6.3 Results ……41
6.3.1 BiAb armed CD34+ cells preserve heart function comparable to direct injection ……41
6.3.2 BiAb homed CD34+ cells reduces infarct size comparable to direct injection ……45
6.3.3 BiAb targeted CD34+ cells promote angiogenesis and uniform neovascularization ……46
6.4 Discussion ……49
Chapter 7: Effect of BiAb armed HSCs on electrophysiology ……52
7.1 Introduction ……52
7.2 Methods ……...53
7.2.1 Rat acute MI model ……53
7.2.2 Arming of human CD34+ cells ……54
7.2.3 Administration of CD34+ cells ……54
7.2.4 Echocardiography ……54
7.2.5 Optical Mapping ……54
7.2.6 Pacing protocol ……55
7.2.7 Data analysis ……56
7.3 Results ……56
7.3.1 Echocardiography ……....56
7.3.2 Ventricular tachycardia inducibility ……57
7.3.3 Electrophysiological alteration in MI ……57
7.3.4 Different CV in MI in different groups ……...58
7.3.5 Treatment effect on APD ……59
7.4 Discussion ……..…60
Chapter 8: Time series analysis of optical mapping data in MI rat ……..…63
8.1 Introduction ……..…63
8.2 Time domain analysis ……64
8.3 Complex demodulation analysis ……67
8.4 Residual from complex demodulation was an AR process of order 6 to 7 ….75
8.5 Discussion ……...77

Chapter 9: Conclusion 79
Reference.. 81

Chapter 1:

Introduction

1.1 Coronary heart disease, myocardial infarction and cardiac arrhythmia

Coronary heart disease (CHD), as the largest contributor to premature mortality in the United States affacts an estimated 60 million patients and costs the healthcare system approximately $186 billion annually[1, 2]. CHD starts from the formation of thrombus from plaque rupture in coronary vessels, further leads to an acute reduction of blood supply to myocardium, and eventually causes myocardial infarction (MI), the rapid development of myocardial necrosis due to a critical imbalance between oxygen supply and demand of the myocardium [3]. As estimated, 1,100,000 Americans will suffer from a new or recurrent MI every year with over a 45 percent mortality rate in the first year [1, 2]. Surviving patients are often left with severe myocardial damage resulting in debilitating congestive heart failure due to the very limited regenerative ability of cardiomyocytes. Heart transplantation is the only successful treatment for end-stage heart failure; however, the ability to provide this treatment is limited by the availability of donor hearts [4, 5]. Nearly 1900 Americans die of ischemic heart disease everyday, an average of one death every 45 seconds. Worldwide, cardiovascular diseases claim 12 million deaths annually about as many lives each year as cancer, chronic lower respiratory diseases, accidents and diabetes mellitus combined.

Although heart failure results from mechanical dysfunction as the heart is unable to eject sufficient blood to supply the body, in fact, more than half of heart failure patients die of sudden apparent arrhythmias for not fully understood mechanism because maladaptations to MI modify electrophysiology and provide the arrhythmogenic substrate. Therefore, a successful treatment of MI does not only prevent the negative remodeling but also inhibits arrhythmias.

1.2 Pathology and physiology

It is of paramount importance to understand pathology and physiology in order to provide effective treatment. Myocardial infarction occurs when myocardial ischemia exceeds a critical threshold and overwhelms myocardial cellular repair mechanisms that are designed to maintain normal operating function and hemeostasis. During a MI, cardiomyocytes undergo necrosis. Subsequently, macrophages, monocytes, and neutrophils migrate into the infarct area, initiating the inflammatory response and formation of granulation tissue around the necrotic tissue [6-8]. Fibroblasts infiltrate the infarct area and secret matrix metalloproteases (MMPs). Under the effect of MMP, the extracellular matrix is degraded, causing myocyte slippage at the border of the MI leading to ventricular wall thinning and ventricular dilation. At the end of the inflammatory response, non-conductive scar tissue forms as cardiomyocytes in the boarder zone undergo apoptosis and myocardial fibrosis occurs in both the infarcted area and noninfarcted boarder zone [9], and results in non-uniform electrophysiological properties. Meanwhile, the vasculature in the infracted area changes as the number of vessels decreases and the size increases[10]. In summary, the negative remodeling

process of the left ventricle following a MI includes loss of cardiomyocytes, change of vasculature, modification of the extracellular matrix (ECM) and creation of arrythmogenic substrate. This irreversible negative modeling process, contributes to left ventricular dilatation and leads to congestive heart failure.

1.3 Current Treatments

Current therapeutic approaches include pharmacological therapies, mechanical devices and surgeries [11, 12]. Pharmacological therapies can be categorized by effects to three types as, 1) preventing the formation of thrombus through anti-thrombotic agents such as aspirin and heparin to inhibit platelet function by blocking cyclooxygenase and subsequent aggregation; 2) decreasing preload and afterload by the use of vasodilators as nitroglycrin to counteract coronary artery spasm and increase coronary blood flow; 3) blocking beta-adrenergic stimulation to inhibit chronotropic, inotropic, and vasodilatory responses, so that blood pressure is reduce and in turn, decreases myocardial oxygen demand [13]. Depending on the severity of a patient's condition, therapeutic options include administration of an intravenous thrombolysis, percutaneous coronary intervention, known as balloon angioplasty, to reestablish coronary perfusion based on catheter-technology, or coronary artery bypass graft [14]. As stated at the beginning, heart transplantation is the only successful treatment for end-stage heart failure while patients may wait for years for a donor heart. Therefore mechanical devices are used clinically as an alternative to heart transplantation. Mechanical devices include constraint devices (CorCap™) which only provides external support by an implanted mesh wrap around the heart without repairing the injury, and artificial hearts (AbioCor TM) which is

only designed for patients without alternatives. In summary, there is no cure for MI and the development of other strategies is needed.

1.4 Bioengineering approaches in cardiac research

As an interdisciplinary subject, bioengineering is an area utilizing engineering breakthroughs, implementing engineering approaches to understand mysteries and solve problems in biology and medicine. This also brings new viewpoints for cardiac research.

1.4.1 Cell therapy

For over a decade, the possibility of cell transplantation for myocardial regeneration and repair has been investigated. Issues common to all cell types used for cardiac repair are survival of engrafted cells, differentiation, host tissue-transplant cell interactions, and electromechanical coupling[15]. A variety of cell types have been reported to be beneficial in myocardial repair. This has led investigators searching for "the best cell type for myocardial regeneration".

Cell types including fetal, neonatal, and adult cardiomyocytes[15], skeletal myoblasts[16], bone marrow progenitors cells[17] and embryonic stem cells [18, 19] have been considered for cardiac repair. Adult cardiomyocytes were unable to survive even when transplanted into normal myocardium. Both fetal and neonatal cardiomyocytes were able to form viable grafts as well as express cadherin and connexin 43 (gap junction protein in cardiomyocytes), which are necessary to form electromechanical junctions[20]. Although the fetal and neonatal cardiomyocytes were able to form these junctions, they

are currently not a feasible source of transplant cells due to the many ethical and donor availability issues. Cardiac stem cells are the perfect candidate for MI repair, but they are limited in number within the myocardium and are currently difficult to expand. Embryonic stem cells injected post-infarction have been shown to produce long-term improvement in cardiac function over 32 weeks[18]. However, the difficulty in amplifying the cells in culture, the possibility of feeding layer contamination of human embryonic stem cell lines, potential for teratoma formation and ethical concerns have limited the use of embryonic stem cells. Skeletal myoblasts, on the other hand, are not subject to such ethical issues. These cells may be isolated from a muscle biopsy and subsequently expanded *in vitro*. They have been shown to survive and form intercalated discs in myocardium[16]; however, they do not form gap junctions and thus it is unlikely that they contract synchronously with the surrounding cardiomyocytes[21]. Recent clinical trials have demonstrated modest improvements in left ventricular function and a low incidence of hospitalizations for heart failure patients[22, 23]. However, electrical instability has been seen in some patients transplanted with skeletal myoblasts. Therefore, use of skeletal myoblasts for cardiac repair may be limited[16].

Human bone marrow derived G-CSF mobilized CD34+ cells were shown to induce vasculogenesis and angiogenesis in rat MI and recover left ventricle (LV) ejection fraction (EF) by 22%[24]. Orlic et al reported myocardium regeneration, new vessel formation, and further cardiac function improvement and decreased mortality by the use of c-kit+, lin- bone marrow derived stem cells in an allogeneic mouse model with total ligation of left anterior descending artery (LAD)[25, 26]. Other studies have also

reported functional improvement and cell transdifferentiation into cardiomyocytes, smooth muscle cells and endothelial cells[27]. These studies have shown hematopoietic stem cell (HSCs) transplantation improves cardiac function. More studies were designed to explore the mechanism behind the improvement in cardiac function and the cell fate after transplantation. Most of the transplanted hematopoietic stem cells remained undifferentiated in the infarct, some differentiated into endothelial phenotype (3.3%), and very few differentiate into cardiomyocyte phenotype (0.02%) which is about the same rate as cell fusion[28]. Other studies showed that hematopoietic stem cells are unable to transdifferentiate into myogenic cells but retaining the hematopoietic fate in a mouse model[21, 29, 30]. A putative conclusion is HSCs improve cardiac function through a paracrine effect. This notion is supported by VEGF overexpressed stem cells enhancing the improvement more than the wild type in rat MI[31]. Therefore, explanations based the revascularization in the infracted area and/or paracrine effects are better accepted.

Clinical studies have substantiated preclinical reports that hematopoietic stem cells improve myocardial function following an ischemic insult [32, 33]. Academicians and industry groups have demonstrated the feasibility of harvesting hematopoietic stem cells from cardiac patients [34-37]. Despite these encouraging advances, advocates recognize variability in clinical response with potential major limitations due to insufficient homing and retention of stem cells within the injured myocardium [38]. An efficient delivery method is needed for the success of cardiac stem cell therapy.

Stem cells have been administered systematically, intracoronary, or directly injected into the myocardium in most of the cellular cardiomyoplasty studies. Although positive results have been observed, the accumulation of transplanted cells in other organs as lung[39], cell death because of an unsuitable milieu and poor retention in long term are issues which need to be addressed to increase the efficacy of stem cell therapy.

1.4.2 Antibody targeting technology

Our lab pioneered homing stem cells to myocardial injury by the use of antibody targeting technology [40, 41]. The idea of antibody targeting is adapted from cancer research area where T-cell or other immune cells are redirected to antigen-specific tumor target[42]. The basic principle is to conjugate an antibody to a unique antigen expressed in the infarct area with another antibody to a surface antigen of the targeted cells. Bispecific antibodies (BiAb) will direct the cells to the infarcted area instead of other organs. This method not only improves the efficiency of cell delivery but also distributes the cells more uniformly in the myocardial infarct, providing a more favorable milieu than direct injection of large amount of cells in one or several spots.

Successful repeatable animal trials from our and other groups verified the concept and efficacy of BiAb technology. As early as 2003, successful homing of Lin-Sca+ murine stems cells to MI was reported in mice by the aid of anti-c-kit x anti-VCAM-1 BiAb as VCAM-1 adhesion molecules are upregulated in on injured cardiomyocytes [40]. Later, our lab further reported that anti-CD45 x anti-cardiac myosin light chain (CD45 x MLC) BiAb not only targeted human CD34+ stem cell to myocardial injury but also preserved

cardiac function compared to unarmed cells. The homed human CD34+ stem cells were incorporated in myocardium and vessels [41]. Zhao et al observed similar results in mice with CD45 x MLC armed human CD34+ stem cells [43]. Unpublished data from our lab shows that such antibody targeting approach is as effective as direct injection of the same amount of cells to MI and lowers the ventricular tachycardia inducibility.

1.4.3 Biomaterials

A range of materials from synthetic materials such as polyglycolic acid, polylactic acid or polyethylene glycol to biological materials such as gelatin, collagen or matrigel have been used for myocardial repair [44]. Biopolymer matrices are expected to have similar structural characteristics to biological tissue and degrade over time in order to provide the matrix for new tissue formation. In contrast to a bioengineered cardiac graft, the injectable scaffolds remain in liquid form until after injection. After *in vivo* solidification, the engineered biopolymer matrices have the potential to provide mechanical support, promote cell migration and proliferation and angiogenesis. The appropriate material for the myocardial repair should be mechanically robust but also pliable and provides a physiological environment for cardiomyocytes.

Chapter 2:

General Methods

2.1 Introduction

This chapter introduces the methods used in the studies reported. These methods include the creation of the rat model of ischemia-reperfusion MI, in vivo measurement of cardiac function by echocardiography and histological procedures.

2.2 Rat acute myocardial infarct model and cell administration

All surgical procedures were approved by the Committee for Animal Research of the University of California San Francisco and performed in accordance with the recommendations of the American Association for Accreditation of Laboratory Animal Care. The ischemia reperfusion model has been extensively tested in our laboratory for almost twenty years [45]. The female immnodeficient nude rats (200-250g) were intubated endotracheally, connected to a rodent ventilator (Harvard Apparatus), and anesthetized by inhalation of 2% isoflurane. A median sternotomy was performed, and left anterior descending coronary artery (LAD) was occluded with a single stitch of 7-0 Ticron suture for 17 or 25min, and then reperfused. The chest was then closed, and the rat was allowed to recover. Twenty-four to forty-eight hours after myocardial injury, rats were treated by direct injection of cells into the MI, intravenously administered cells or PBS as control.

Intravenous injection: Armed or unarmed 2M cells in 0.25cc PBS or 0.25cc PBS only were injected intravenously via either jugular vein when rats were anesthetized by isoflurane and then recovered.

Direct injection guided by high-resolution echocardiography: Echo-guided direct injection was well established in mice [46] and we here approached similarly in rats. Echocardiography was accomplished with Vevo 660 system (VisualSonics, Toronto, Canada). A 50µl Hamilton syringe was loaded with 2M cells in 50µl PBS, secured in a micromanipulator and aligned with the scan head probe such that the needle could be viewed under echocardiography. The needle was then advanced with the micromanipulator through the body wall and diaphragm until the needle bevel in the center of the hypokinetic part of LV free wall under the echo guidance. The cells or PBS only will be injected in the injured region.

2.3 Echocardiography

Transthoracic echocardiography [47] was performed with a 15-MHz linear array transducer system (Sequoia c256, Acuson) on all animals consciously or under anesthesia by inhalation of 2L/min isoflurane at different time points including before cell injection and at end point. The anesthesized animals were placed in a prone or slightly lateral decubitus position while the conscious animals were placed in a decap cone. Then a layer of acoustic coupling gel was applied to the thorax. Two-dimensional images were then obtained in both parasternal long- and short-axis views at the papillary muscle level. Enhanced resolution imaging function (RES) was activated with a region of interest adjusted to heart size whenever possible. The gain was set for best imaging, and the compression was

set at 70 dB. Two criteria were used for adequate imaging. First, the short-axis view must demonstrate at least 80% of the endocardial and epicardial border. Second, the long-axis view must demonstrate the plane of mitral valve, where the annulus and the apex could be visualized. With sufficient two-dimensional image slips, then the M-mode images were obtained and the wall thickness and LV internal dimensions (LVD) were measured according to the leading edge method of the American Society of Echocardiography. Fractional shortening (FS) as measure of systolic function was calculated from LVD in diastole and systole (FS=(LVDd-LVDs)/LVDdX100%), where LVD for the left ventricular internal dimension, d for diastole and s for systole. The echocardiographer was blinded to the treatment groups during the data acquisition and analysis. Our previous studies and other reports have demonstrated the accuracy and reproducibility of transthoracic echocardiography in rats with myocardial infarcts.

2.4 Tissue collection and fresh frozen sectioning

At the end of studies, animals were euthanized with intraperitoneal injection of an overdose of pentobarbital (200 mg/kg) and the hearts were rapidly excised for histology or underwent optical mapping (details in chapter 6). The hearts were harvested, then trimmed off atria and aorta, and fresh frozen in O.C.T. freezing medium (Sakura Finetek) at -20°C.

The frozen hearts were sectioned into 10μm slices by Microm HM 500 crystat (Richard-Allen Scientific) and 10 consecutive sections (2sections per slide) were collected to charged glass slides in every 35-40 sections throughout the MI region [48].

2.5 Histochemical assessment

For each experiment, typically ten representative slides were stained with hematoxylin and eosin (H&E, Fisher Scientific) and Masson's Trichrome stain (Accustain, Sigma) for histological analysis.

Hematoxylin and eosin stain procedure: a) heart slides were rinsed in distilled water, b) dipped in Harris Hemotoxylin for 3 minutes, c) rinsed 3 times in tap water (the following rinsing steps were the same), d) dipped in bluing solution for 1 minute, e) repeat c, f) incubated in Eosin for 30 seconds, g) dehydrated in 95%, 100%, and 100% ethanol for 1minute each, h) finally incubated in SafeClear for at least 1 minute and mounted with Permount.

Masson's Trichrome stain procedure: a) heart slides were incubated overnight in Bouin's solution, b) washed in running tap water to remove yellow color thoroughly, c) dipped in iron Hematoxylin solution for 5 minutes, d) rinsed in tap water then deionized water, e) stained in Biebrich scarlet-acid Fucshin for 5 minutes, f) rinsed in tap water then deionized water, g) then placed in Phosphotungstic/Phosphomolybdic acid solution for 5 minutes then another 5 minutes in Aniline blue solution, h) dipped in 1% acetic acid for 2 minutes, and i) finally rinsed, dehydrated and mounted.

The infarct size was traced in H&E stained slides as published previously [49] and was reported as percent infarct area of left ventricular area. The fibrosis was reported from Masson's Trichrome stain as blue region in the infarcted region.

Chapter 3:

Bispecific Antibody

3.1 Introduction

The concept of a magic bullet, which describes the idea of specifically targeting a therapeutic agent to the desired tissue, is more than a great concept after the tremendous advances in monoclonal antibody (mAb) technology. The success of this strategy is expanded by the conjugation of two mAbs into one bispecific antibody (BiAb) which has the specificity of both mAbs and allows redirecting of therapeutic agents to tissue specific antigen. The BiAb strategy has been successfully adopted to kill tumor cells by targeting immune cells [42].

This concept has also gained more and more attention along with the surge of cell transplantation for cardiac repair as the efficiency of therapeutic cells homed and retained in the MI is dependent on the efficacy of such therapies [40-43, 50]. A BiAb with one mAb specific to antigen only expressed in injured myocardium is able to guide the therapeutical cells to MI and enhance the homing efficiency. We developed anti-CD45 x anti-MLC (CD45 x MLC) BiAb which chemically conjugated two monoclonal antibodies, anti-CD45, the common leukocyte antigen on human hematopoietic stem cells, and anti-cardiac myosin light chain (anti-MLC), an organ specific injury antigen expressed in infarcted myocardium.

In order to characterize conjugated CD45 x MLC BiAb, a binding curve of efficiency at different BiAb concentrations was obtained by measuring the percentage of cells with positive staining of the isotype of anti-MLC. The result provides an optimal arming concentration and procedure for future animal studies. In this study, the successful binding was demonstrated and quantified by flow cytometry.

3.2 Methods

3.2.1 Conjugation of bispecific antibody

The conjugation of BiAbs was schematically shown in figure 3.1. Briefly, 1mg mouse IgG1 anti-human CD45 (BD Pharmingen) in 50mM NaCl, 1mM EDTA, pH8.0 was reacted with a 10-fold molar excess of Traut's reagents (2-iminothiolane HCl, Pierce) and 1mg mouse IgG2a anti-MLC(Abcam) in 0.1 sodium phosphate, 150mM NaCl, pH7.2 is reacted with a 10-fold molar exess of Sulfo-SMCC (sulphosuccinimidyl 4-(N-maleimidomethyl) cyclohexane-1-carboxylate, Pierce) respectively at room temperature for 1 hour. After eluting from desalting columns to remove unlinked Traut's reagent and Sulpho-SMCC, the chemical-linked antibodies were mixed at equal molar ratio to form heteroconjugation at 4°C overnight to produce anti-CD45 X anti-MLC (CD45 X MLC). A nonreducing SDS-PAGE gradient gel was run on the final product and stained with Coomassie blue.

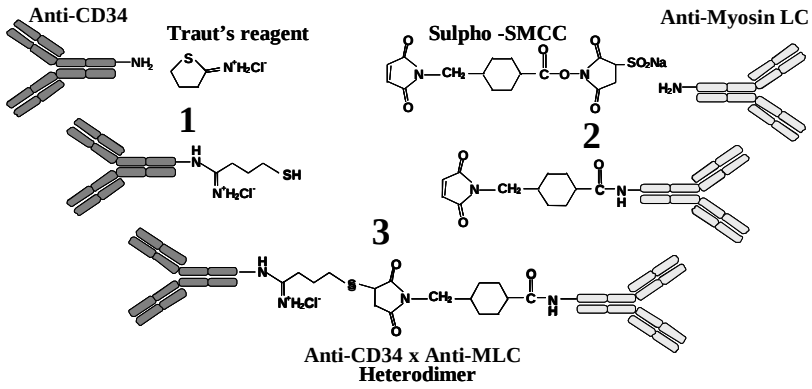

Figure 3.1: Construction of Bispecific Antibody

3.2.2 Flow cytometry

Frozen human CD34+ cells (Cambrex, now Lonza) were recovered in media and counted. Then the cells were armed with at 0 (negative control), 0.01, 0.05, 0.25, 1, 4, 16, 64, 256 µg/ml CD45 x MLC BiAb in a volume of 50µl with 5 million cells/ml. The CD34+ incubated with CD45 x MLC BiAb for 15min at room temperature and then washed twice by spinned down and resuspended in PBS. CD45 X MLC armed CD34+ cells were incubated with anti-mouse IgG2a+b PE (BD 340269, 20µl/test, 0.0015mg/ml) or IgG isotype control antibodies and then subjected to flow cytometry (BD FACSCalibur).

3.3 Results

3.3.1 Conjugation of CD45 x MLC BiAb

The SDS-polyacrylamide gel electrophoresis picture was shown in figure 3.2. From the gel picture, it could be seen that the heteroconjugation product was a mixture with different molecular weight. As the molecular weight of mouse IgG (both IgG1 and IgG2a) is about 150 kilo Dalton (kDa), the bands around 150kDa were monomers, the bands around 300kDa were dimmers, and the bands with higher molecular weights were

multimers. The heteroconjugation product contained unreact monomers, useful dimmers, and mulimers.

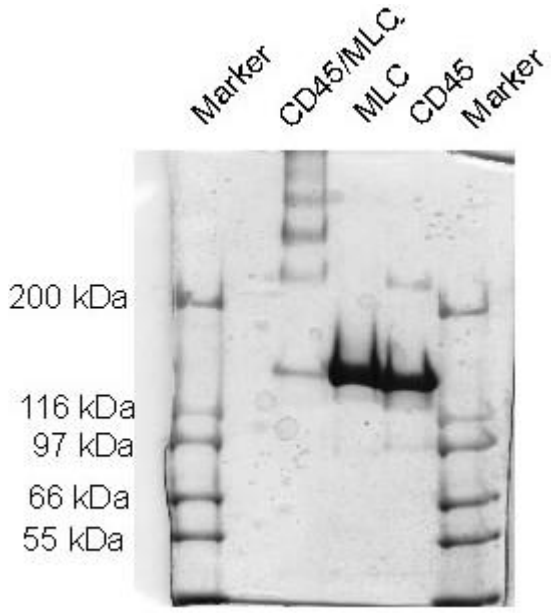

Figure 3.2 SDS-polyacrylamide gel electrophoresis showed markers (lane 1), hereteroconjugation product (lane 2), Sulfo-SMCC linked anti-MLC (lane 3), Traut's linked anti-CD45 (lane 4), markers (lane 5). The bands around 150kDa were monomers, around 300kDa were dimmers, and higher than 300kDa were multimers.

3.3.2 CD45 x MLC binding efficiency curve

The BiAb binding efficiency on CD34+ cells are dose-dependent. Percentage of mouse IgG2a (isotype of anti-MLC) positive cells increases as arming BiAb concentration increases and plateau at concentrations greater than 16μg/ml at which 95% cells are positive with anti-MLC (figure 3.3a). The median fluorescence intensity plateau at a higher concentration around 16μg/ml (figure 2b) because the surface binding sites of a cell, CD45, is not saturated with CD45 x MLC BiAb when the cell just showed mouse IgG2a positive. Therefore, there were still binding sites for CD45 x MLC BiAb and

when all the binding sites were saturated with more BiAb, there were more mouse IgG2a binding and so increased the fluorescence intensity.

According to this result, CD34+ cells were armed at 0.5µg/M cells with 16 million cells/ml for the in vivo studies. Flow cytometry after cell injections showed that more than 90% CD34+ cells are armed with CD45 X MLC BiAb (figure 3.3c) while the unarmed cells are all negative in mouse IgG2a (figure 3.3d).

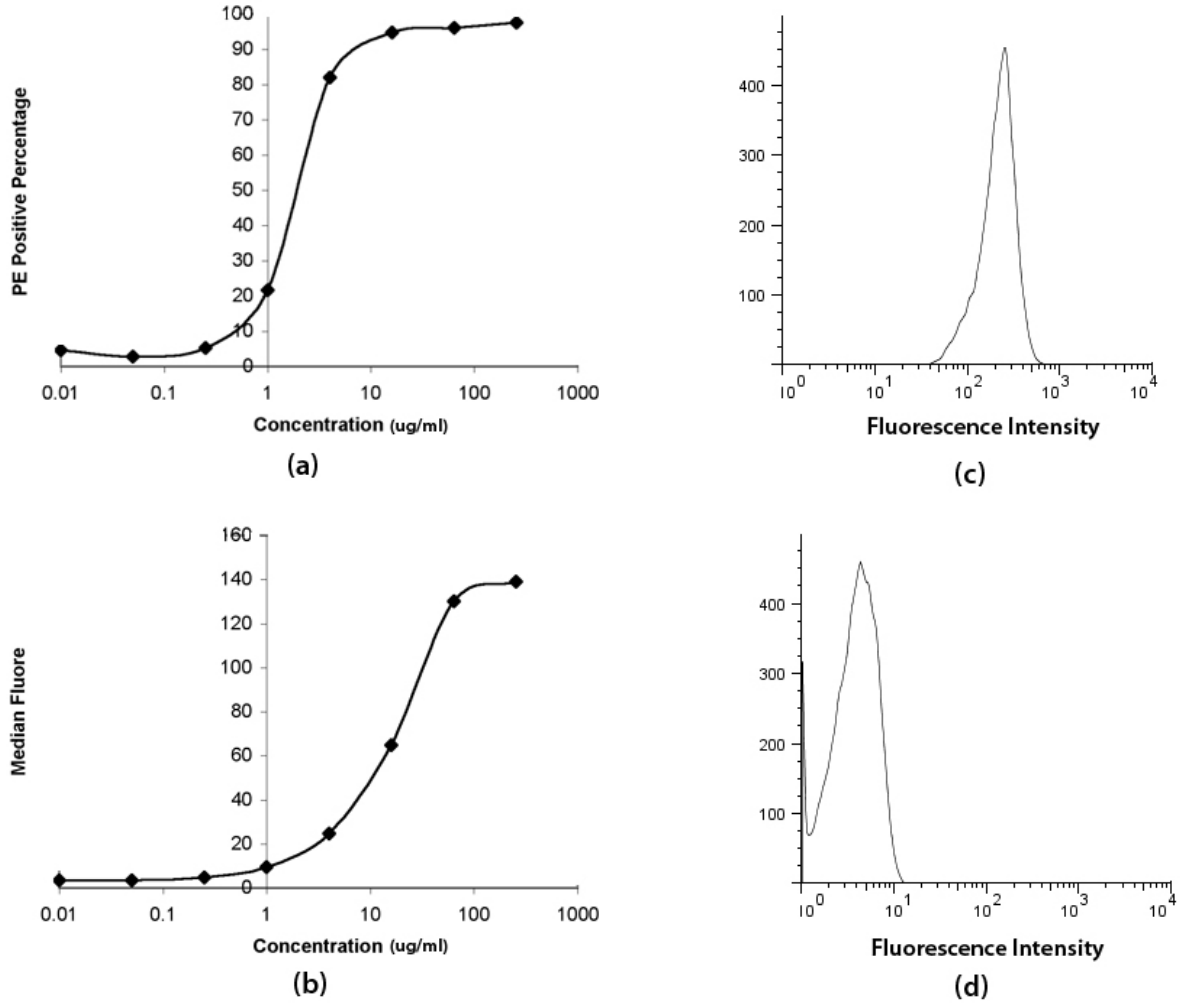

Figure 3.3: The optimal arming BiAb concentration is decided based on BiAb binding efficiency. Percentage of cells with positive stain of CD45 X MLC BiAb is increased as

the BiAb concentration increases during arming and 95% cells are positive at concentrations higher than 16μg/ml (a), while the median fluorescence intensity is saturated at higher concentration (greater than 64μg/ml, b) because positive stain of mouse IgG2a indicates the binding of BiAb but not saturation of cell surface binding sites (CD45). The cells armed at 8μg/ml are almost all positive in mouse IgG2a (c) comparing to the unarmed cells (d).

3.4 Discussion

This study demonstrated the successful linking of cardiac injury specific antibody to human CD34+ cell. Moreover, it quantified the binding kinetics and served as a guideline for future studies. To our knowledge, this is the first study to exam BiAb binding efficiency on stem cells in vitro. One concern with BiAb is from chemical conjugation with extra molar cross-linkers like Traut's and SMCC as the cross-linkers are not specific to amino groups at the end of peptides. The cross-linkers can react with amino acid residuals containing amino groups in the side chain such as Arginine, Asparagine, Glutamine and Lysine. An over cross-linked antibody will change its conformation and may lose the motif for specific binding. Therefore, a flow cytometry test in this study only demonstrated that the motif to CD45 was functional after heteroconjugation. This test did not prove that the specificity at anti-MLC end is intact and able to bind to myocardial injury although the monoclonal anti-MLC was linked to human HSCs. This has to be tested in vivo as the cells shown in MI. In future, an ELISA-like study can be performed for in vitro testing by coating cardiac MLC protein on plates and observed whether the CD45 x MLC armed human CD34+ cells binds. We

did not perform this test because 1) commercially available cardiac MLC protein is very expensive and 2) we verified this in vivo.

Chapter 4:

Detection of BiAb homed stem cells with MRI

4.1 Introduction

Human CD34+ cells can be targeted to injured myocardium when armed with CD45 x MLC BiAb through intravenous injection in a rodent model of ischemia-reperfusion induced myocardial infarction [40, 41, 43]. Despite the functional improvement during the course of the study, there were a few detectable cells after 5 weeks and almost no cells left after 3month [41, 51]. Moreover, the detection of the cells is by end point histological analysis, and it is expensive to determine the role of stem cells in preventing negative remodeling by sacrificing animals at different time points and hard to draw statistical conclusions. Therefore, a tool able to detect cells *in vivo* will help to explore the cell fate, migration after administration, and further understand the mechanism of the beneficial effect of stem cells in treating MI although they all disappeared eventually. Superparamagnetic iron oxide (ferumoxides, SPIO), a magnetic resonance image (MRI) contrast agent, was reported to label various mammalian and stem cells successfully without affecting cell proliferation and viability [52].

In this study, we evaluated the effect of SPIO on human stem cells for two weeks, detected SPIO labeled stem cell in myocardium through direct injection or homing. We used human mesenchymal stem cells (hMSCs) for cell viability and proliferation test because human CD34+ cells' proliferation is very low. Prussian blue staining detected

loaded iron particles in SPIO labeled hMSCs for at least 14 days. CD45 x MLC BiAb armed CD34+ cells were incubated with ferumoxide-contained media before intravenous injection into a myocardial infarct rat. The animal was imaged 2 days after injection and the heart was harvested immediately after imaging. Prussian blue staining was applied on the frozen sections and verified the existence of iron.

4.2 Method

Rat MI model and cell administration were described in chapter 2.

4.2.1 Cell labeling

Cell labeling method is from Arbab et al [53]. Briefly, poly-L-lysine (PLL, Sigma-Aldrich P4707), stock solution of 1.5mg/ml, was used as transfect agent in cell labeling. PLL stock solution was added to the culture media at a dilution of 1:1000 and mixed with ferumoxides (Berlex 59338-7035-5) contained culture media (50μg/ml) at room temperature for 60 minutes on a rotating shaker. The mixture was added to hMSCs or human CD34+ cells (Cambrex, now Lonza) and kept overnight at 37°C with 5% CO2. The mixture was removed the next day and the hMSCs were cultured in normal culture media on chamber slides while the armed CD34+ cells were washed by spinning down and resuspended in SPIO-free media for BiAb arming.

4.2.2 Arming of human CD34+ cells

CD45 x MLC BiAb was produced as in chapter 3. SPIO-labeled human CD34+ cells were washed and reconstituted to 16million cells/ml and armed with CD45 x MLC BiAb at 0.5μg/M such that the BiAb concentration was 8 μg/ml and the arming efficiency was

above 90% according to titration from chapter 3 (Chapter 3, figure 3.1). The cells were incubated with the BiAb for 15min at room temperature and then washed twice by spinned down and resuspended in PBS for further injection.

4.2.3 Prussian blue staining of iron particles

Cultured hMSCs were collected 1, 2, 4, 6, 13 days and then fixed by 4% Glutaraldehyde. The rats receive SPIO labeled cells were sacrificed and theirs heart were fresh frozen and sectioned accordingly. The sections were also fixed by 4% Glutaraldehyde. Prussian blue staining was used to detect iron particles. The fixed slides were washed and incubated with 2% potassium hexacyanoferrate (Sigma P9387) and 6% hydrochloric acid (Fisher A144-212) for 30 minutes to stain iron oxide and then followed with H&E staining.

4.3 results

4.3.1 Iron-labeled cells are detectable under MRI

The hMSCs from different time points (figure 4.1 a-e) were stained with Prussian blue followed with H&E staining to characterize the effect of ferumoxide on the human stem cells. The blue dots in the cytoplasm indicate the iron particle inside the cells. The iron particles located only in cytoplasm not in nuclei at all. The hMSCs proliferated at the same rate as non-labeled cells. The center cell in figure 4.1 b was dividing as two nuclei in this cell. SPIO was diluted as the time went. This might be explained by cell secretion of SPIO particles similar to exocytosis, or dilution from cell growth and cell proliferation, and so forth.

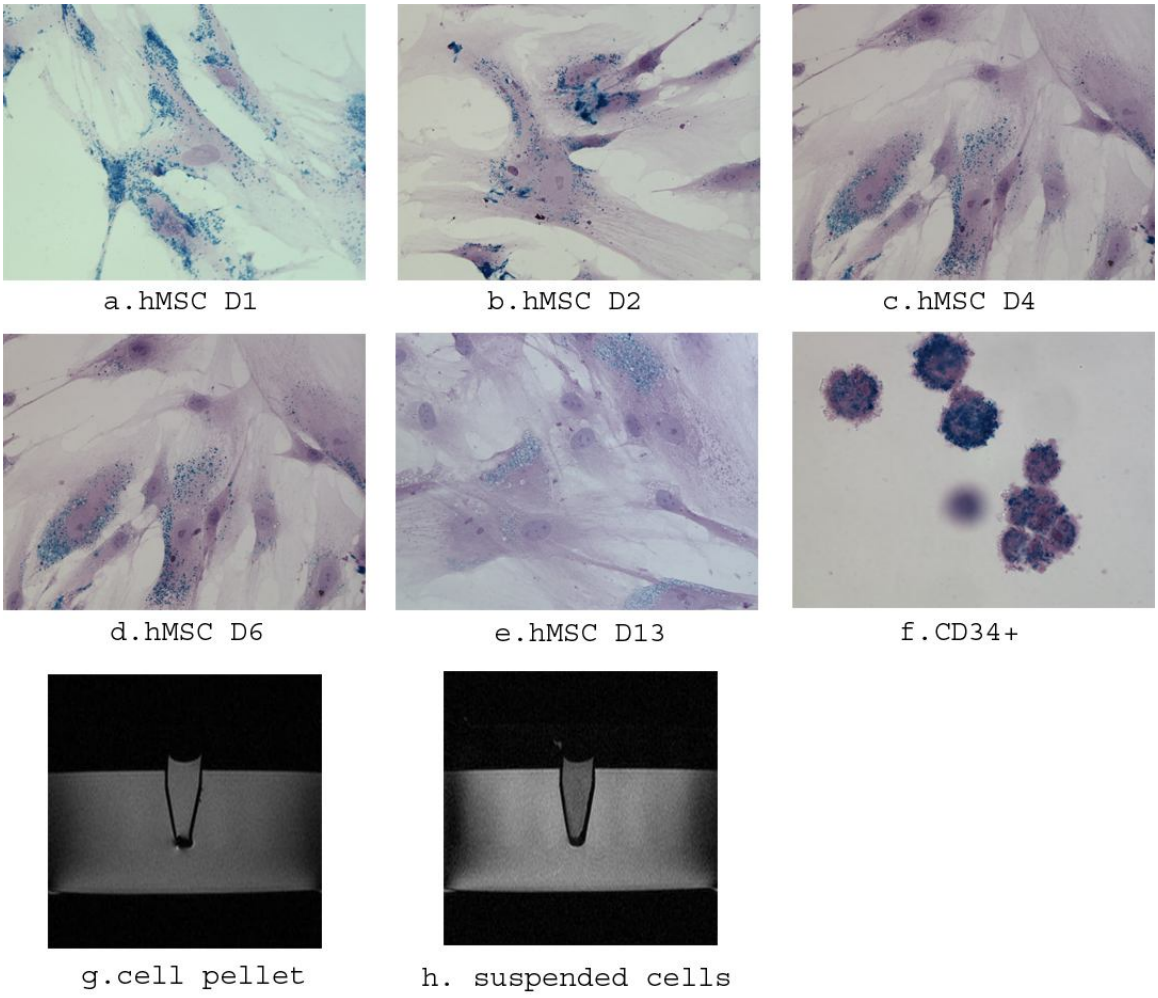

Figure 4.1 Iron labeled hMSCs at different time point (a-e) under 40X objective, right after removing the ferumoxides-contained media and washed with PBS (a), day 2 (b), day 4 (c), day 6 (d), and day 13 (e). Iron is diluted due to proliferation and cell growth. Iron labeled CD34+ cells on day 1 are under 60X objective. Day 1 iron labeled hMSC is imaged with MR as a cell pellet (g) or suspended cells in an Eppendorf tube (h). The strong signal in g shows distortion at the tip.

The CD34+ cells are only stained on the first day of labeling (figure 4.1 f) to verify successful labeling. MR imaging of SPIO-labeled hMSCs in Eppendorf tubes (figure 4.1 g, h) showed the successful labeling of the cells. The signal of the SPIO-labeled cells was very strong under 2T so that distortion of image was observed (figure 4.1 g) when cells aggregated to a pallet.

4.3.2 SPIO-labeled homed cells were correlated in histology and MRI

Two days after occlusion, 2M CD45 x MLC BiAb armed human CD34+ cells labeled with SPIO were injected through jugular vein. One day after injection, the animal was imaged and the heart was harvested right after imaging. The heart was sectioned at 10μm from apex to base and the tissue was stained with Prussian blue as well as HE.

The infarct area were along the LV free wall toward the interventricular septum (figure 4.2 a). The iron positive cells were only distributed in the infarct area (figure 4.2 a) because BiAb binding leads the CD34+ cells to injured area where myosin light chain was expressed abundantly. At 3 days after occlusion, the injured area was swollen due to the inflammatory process, shown as thickening in LV free in figure 4.2 b and c. The SPIO-positive areas in MR images were at the thickened LV free wall and the junction of the LV free wall and the interventricular septum (figure 4.2 b c, red arrows); b was closer to apex. We surmised that figure 4.2 a showed a position between b and c based on the distribution of iron-positive cell.

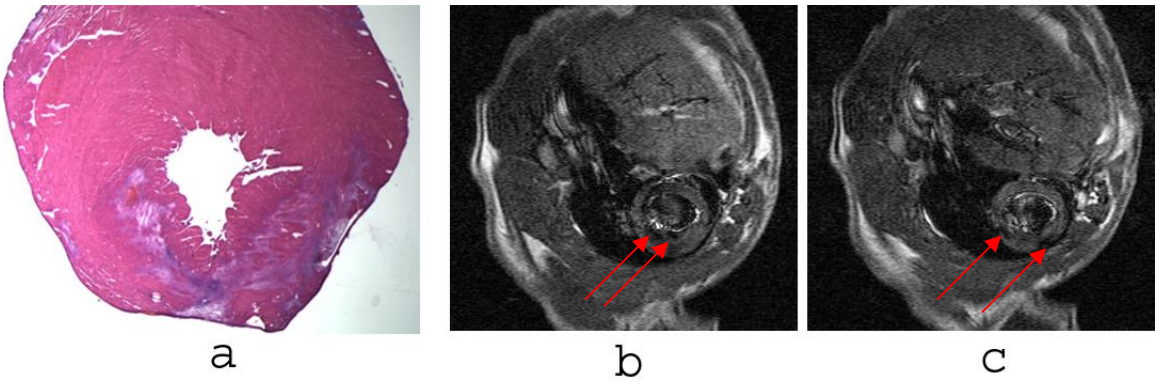

Figure 4.2 SPIO-labeled BiAb aremed CD34+ cells targeted to myocardial infarct. The iron-positive cells only in the infarct area (a). MR imaging of the animal transaction at two levels with the iron positive sites indicated with red arrows (b, c).

4.4 Discussion

BiAb armed human CD34 + cells were targeted into myocardial injury, moreover, the armed cells could be further labeled with SPIO particles and detected under MRI. This result was very encouraging as we could measure heart function with MRI as well so that the therapeutical cells and the cardiac function could be observed under one frame work. However there were several unsolved issues which interfered with positive observations. We did not know the fate of SPIO particle after the death of labeled cells. It would not be a problem if SPIO would be washed off rapidly after cell death. Otherwise, the residual SPIO could be very misleading as we could not differentiate MRI signal loss was due to SPIO in the survived cells or from the dead cell released SPIO. More studies were needed to answer this question and give a clear conclusion. We stopped this study due to the very low survival rates (2 out of 12) after MRI. This low survival rate was from technical reasons including: 1) breathing problems most likely tracheal swelling from the intubations; and 2) hypothermia due to the low temperature needed to obtain a high

quality MRI. The rats with MI were too weak to survive in low temperatures while under anesthesia. Despite all the difficulties, this type of study is going to be very promising once the technique is improved.

Chapter 5:

BiAb armed HSCs preserves cardiac function (published [41])

5.1 Introduction

Advances in cellular cardiomyoplasty and adult stem cell research inspired stem cell therapy in myocardial regeneration. The seminal studies by Orlic et al [54-57] demonstrated the plasticity of hematopoietic stem cell (HSCs) into nonhematopoietic tissues and further repairing injured cardiac tissue. Although the idea of HSCs transdifferentiating to cardiomyocytes were challenged and the mechanism of repairing remains controversy [58], the beneficial effect of stem cell therapy in myocardial regeneration was widely reported from different research groups. The controversy in the mechanism of transdifferentiation or angiogenesis also suggests that environmental clues may play an as important role as the characteristics of HSCs in determining the final fate the transplanted HSCs will adapt to. Suitable local milieu is needed to signal HSCs to undergo transdifferentiation, proliferation, or fusion and in turn, repairs the heart. The success of HSC cardiac regenerative therapy, however, may be limited by the amount of HSCs delivered and retained in the injury site given the current popular systematic administration of HSCs. In order to be a viable clinical treatment for myocardial infarct, new delivery method is in urgent need to be able to direct adequate

amount of HSCs to the injury site without invasive procedures which increase risks for morbidity and mortality.

Bispecific antibody (BiAb) targeting strategy was extensively studied in our lab as an efficient and non-invasive way to home therapeutical cells to MI in nude rats. BiAb is a conjugate of two monoclonal antibodies (mAbs) through chemical crosslink to form a bidirectional antibody bridge between therapeutical cells and MI-associated antigen. In this first study in rat model, we explored the potential of BiAb targeting of human HSCs for myocardial repair with the combination of anti-human common leukocyte antigen, anti-CD45 and anti-cardiac myosin light chain, anti-MLC as discussed in chapter 3 and 4 [41]. As a cytosolic protein in cardiomyocytes, MLC is only exposed to outside during myocardial injury, thus to the MLC x CD45 armed HSCs and this ensures the injury-specific homing.

5.2 Methods

5.2.1 Rat acute MI model

Immunodeficient nude rats received 17 minutes occlusion of left anterior descending port of left coronary artery and then reperfused under anesthesia as chapter 2.

5.2.2 Arming of human hematopoietic cells

CD45 x MLC BiAb was produced as in chapter 3. Purified human CD34+ cells (Cambrex, now Lonza) were recovered and reconstituted to 16million cells/ml and armed with CD45 x MLC BiAb at 0.5μg/M such that the BiAb concentration was 8 μg/ml and the arming efficiency was above 90% according to titration from chapter 3 (Chapter 3, figure 3.1). The cells were incubated with the BiAb for 15min at room temperature and then washed twice through spinned down and resuspended in PBS.

5.2.3 Administration of CD34+ cells

Two days after myocardial injury, 9 rats were intravenously injection of 2M CD45 x MLC armed CD34+ cells, and 8 rats received 2M unarmed cells. The details of administration methods were in Chapter 2.

5.2.4 Echocardiography

Transthoracic echocardiography was performed on all 17 rats in the conscious state; other details same as in chapter 2. Cardiac function was measured before MI, 12 and 35 days

after the MI. The study was concluded after the last echocardiography and the rats were euthanized and the hearts were collected and fresh frozen (chapter 2).

5.2.5 Immunofluorescence staining

A. Staining of vasculatures

Representative slides equally distributed through the infarct were double stained for human leukocyte antigen (HLA) class I and smooth muscle α-actin (SMA). Slides were fixed with 1.5% paraformaldehyde and washed with PBS; then incubate with primary antibodies, mouse IgG1 anti-HLA (BD Biosciences) at 1:200 dilution and rabbit IgG polyclonal anti-SMA (Lab Vision) at 1:300 dilution, for 45minutes; and further detected with secondary antibodies, anti-mouse IgG Alex 488 (Molecular Probes, now Invitrogen) at 1:500 and anti-rabbit rhodamine (Molecular Probes, now Invitrogen) at 1:200.

B. Staining of myocytes

Representative slides were double labeled with anti-HLA and rabbit polyclonal anti-Troponin T (Abcam) at 1:300 dilution and followed the same protocol as staining of vasculature; or triple labeled with anti-HLA, mouse IgG2a anti-Troponin I (Abcam) at 1:200 dilution, and mouse IgM anti-connexin 43 (Sigma Aldrich). In triple staining, biotinylated anti-mouse IgG(H+L) rat adsorbed blocker (Vector Laboratories) was applied after primary antibodies to reduce non-specific binding background; then secondary antibodies, goat anti-mouse IgG1 Alex488 (Molecular Probes, 1:2000), goat anti-mouse IgM Alex 546 (Molecular Probes, 1:2000), goat anti-mouse IgG2a Alex350

(Molecular Probes, 1:200), and TO-PRO-3 iodide (Molecular Probes, 1:2000) for nuclei detection were applied for 30 minutes.

Immunofluorescent microscopy (Nikon Eclipse E800) was used to evaluate the staining.

5.2.6 Statistics

Rats were randomized before study. ANOVA was carried out and the p-value was reported using an unpaired 2-tail t-test.

5.3 Results

5.3.1 CD45 x MLC BiAb armed HSCs prevented negative remodeling

Sequential echocardiograms showed that rats received CD45 x MLC BiAb armed human CD34+ cells had significantly better cardiac function than rats received unarmed CD34+ cells 5weeks after MI (figure 5.1). At 5weeks after MI, the fractional shortening (FS) was highly significantly ($p<0.01$) greater and systolic diameter was significantly ($p<0.05$) less dilated in BiAb armed group than unarmed group. In terms of wall thickness, systolic anterior wall was significantly ($p<0.05$) thicker and also the diastolic posterior wall thickness had significantly ($p<0.05$) less compensatory increase in BiAb armed group than unarmed group.

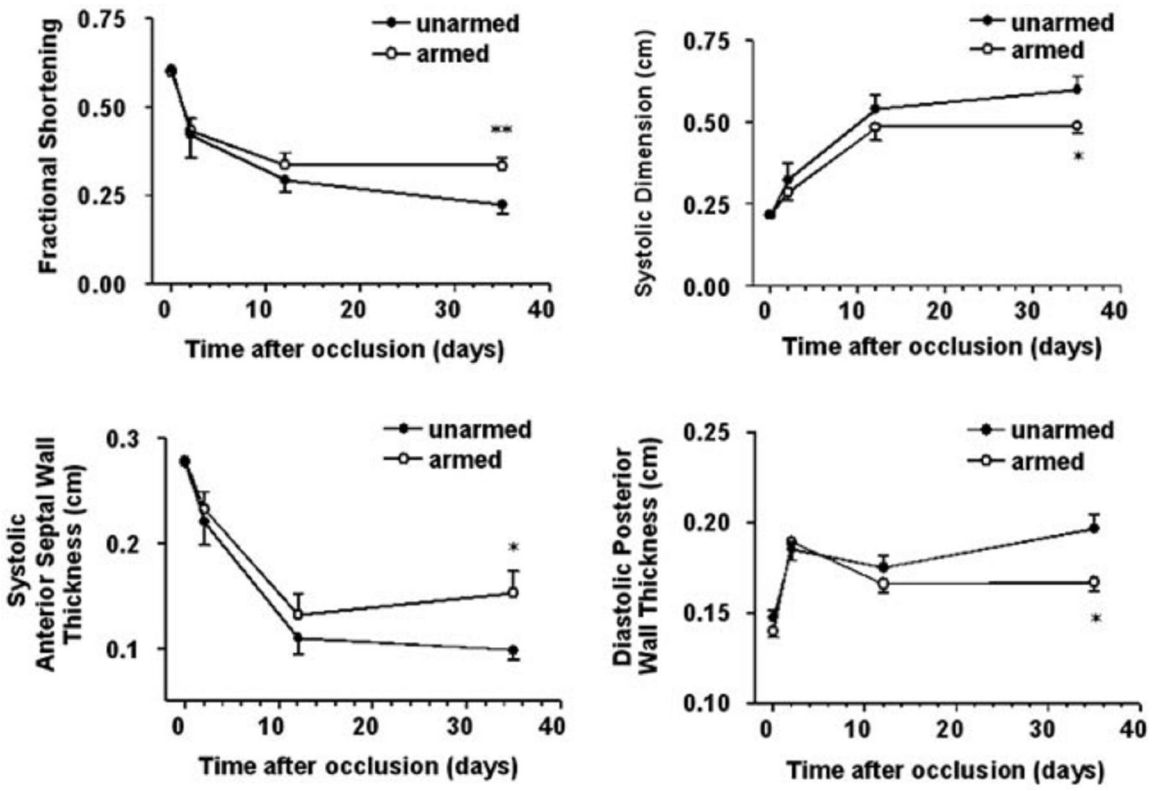

Figure 5.1 BiAb armed HSCs prevented negative remodeling as preserved fractional shortening, less diated systolic dimension, restored anterior wall thickness in systole, and less compensatory posterior wall thickening in diastole. (*: $p<0.05$, ** $P<0.01$)

5.3.2 More HSCs in MI border zone in armed group and coexpress human marker and myocyte specific antigen with gap junction proteins

There were highly significantly ($p<0.01$) more HLA class I positive cells in border and center of MI in the CD45 x MLC armed group (171.8±52.7 cells/high magnitude field, figure 5.2 C) than the unarmed group (<1 cell/high magnitude field, figure 5.2 G). Human HLA and Troponin T double stained cells were detected (figure 5.2 C D) in BiAb armed group and the double stained cells account for about 2.5% of total HLA class I positive cells which was higher than cell fusion rate.

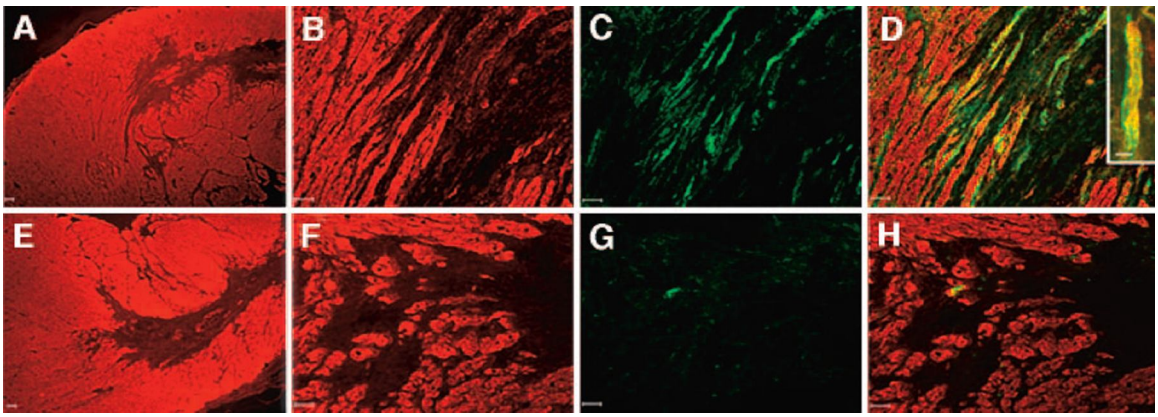

Figure 5.2 Human marker HLA class I and myocyte antigen troponin T were colocalized at MI border zone 5weeks after MI in BiAb armed group (A-D). A lot less cells with positive human markers were found in unarmed group (E-H). Scale bar = 50 μm Staining of troponin T under 40X (A, E) showed MI and healthy region; higher magnification (200X) pictures at border of MI (B, F); staining of HLA in the same view (C, G), the BiAb armed group (C) with a lot more positive HLA staining; merging pictures of B and C (D), F and G (H) respectively demonstrated the colocalization of HLA and troponin T with insert in D shows one representative colocalized fiber under 600X (scale bar =10μm).

Triple label staining demonstrated that the HLA, Troponin I colocalized cells also express gap junction protein connexin 43 between non-HLA positive and HLA positive cells(figure 5.3) and this indicated that the homed cell forms gap junction with native cells. Troponin I was used instead of troponin T in triple staining was because all available mouse anti-troponin T antibody belongs to IgG1 same to the isotype of anti-HLA antibody and unable to be used in triple staining.

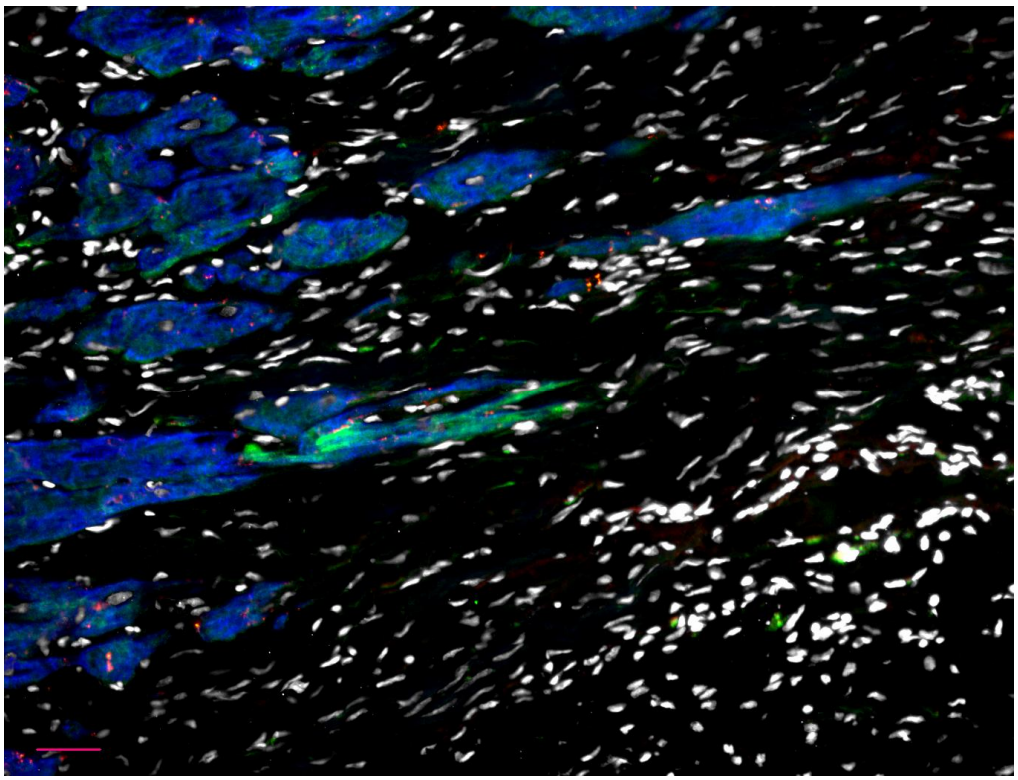

Figure 5.3 Fused/transdifferentiated HSCs also express gap junction protein connexin 43. Troponin I (blue), HLA (green), Connexin 43 (orange), and nuclei (white), 400X, scale bar =10 μm

5.3.3 HSCs may transdifferentiate to smooth muscle cells

Double staining of SMA and HLA class1 demonstrated the colocalization of HSCs and smooth muscle cells (figure 5.4). More HLA positive cells in vasculature than myocytes and it might be more CD34+ cell adopted vascular cell *in vivo*.

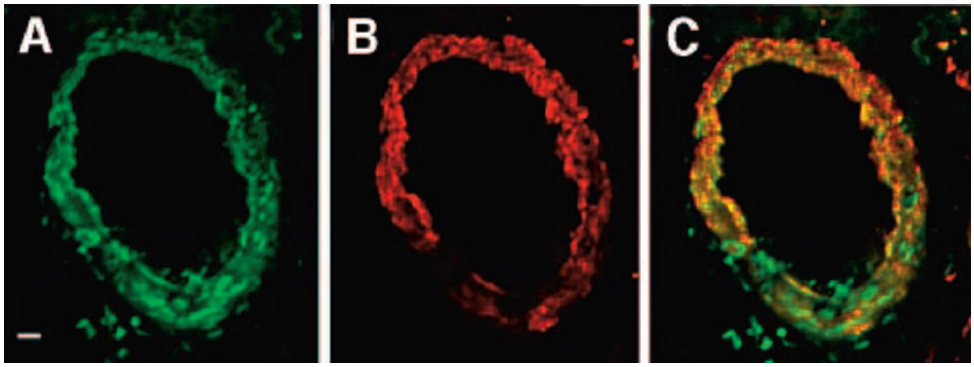

Figure 5.4 Colocalization of human HLA and SMA in a vascular structure in CD45 x MLC armed group. (A) HLA staining, (B) SMA staining, (C) merging A and B. scale bar = 10μm

5.4 Discussion

This study showed that the BiAb homing strategy provided a useful tool for injury specific treatments and demonstrated its power in cardiac stem cell therapy. As a successful homing, CD45 x MLC BiAb redirected more HSCs to MI area and further improved left ventricular function and prevented negative remodeling by keeping contractility, preserving wall thickness, and decreasing ventricular dilation.

However the mechanism of HSCs in treating MI remains unknown and challenges the achievement of tissue repair. In this study, we observed that the homed HSCs adopted different cells fates after infusion, most cells remain undifferentiate, some incorporated in vessels, and some colocalized with myocytes at low rates. HSCs might become to vascular cell type, help the survival of native cardiomyocytes, and improve cardiac function as HLA class I positive cells were seen in vessels. Therefore attenuation of

negative remodeling by neovascularization could be one of reasonable explanations of the beneficial effects from the transplanted human hematopoietic stem cells.

Although the colocalization of myocytes and HLA class I positive cells was very low (2.5%), it was still significantly higher than cell fusion at 0.02% [28]. This indicated that unlike other administration methods, HSCs underwent more than fusion in MI with BiAb homing and this could be explained as homed HSCs were more likely resided in a suitable milieu than other methods. This putative explanation need to be further explored. As most cells did not adopt any cell type, another possible mechanism was paracrine effect or angiogenesis.

No matter which mechanism is proved to be dominant and most beneficial in HSCs treating MI, there is no doubt that more HSCs in MI will magnify the beneficial effects. We observed this from comparison between CD45 x MLC armed and unarmed groups. The antibody targeting of HSCs to ischemic-injured myocardium can be achieved with high specificity, resulting in increased HSC homing and increased numbers of cells that develop into myocyte-appearing cells and localization to vascular structures. In addition, BiAb targeting of stem cells offers a novel noninvasive, nontoxic tool for cardiac stem cell therapy. In order to further demonstrate the advantages of BiAb targeting over other administration method, we need to compare this method with direct injection of HSCs in treating MI.

Chapter 6:
BiAb-homed HSCs preserves cardiac function as efficient as direct injection (Submitted)

6.1 Introduction

Despite recent advances, there is no cure for myocardial infarction (MI) which causes cardiomyocyte death and ventricular negative remodeling. The deterioration in cardiac function leads to congestive heart failure. Due to the very limited regenerative ability of cardiomyocytes, it is impossible to restore myocardium after MI under normal physiological circumstances.

Cellular cardiomyoplasty has ignited enthusiasm of cell therapy by the idea of reconstituting the damaged myocardium with therapeutic cells. Different cell types have been employed to treat MI in animal models with beneficial effects reported[15, 21, 59]. The use of stem cells has blossomed after the report of transdifferention of hematopoietic stem cells (HSCs) into cardiomyocytes [26]. Recently, the idea of transdifferention has been challenged and evidence has shown that the paracrine effect to induce neovascularization is a more plausible explanation for HSCs [29, 58]. Despite the controversy in mechanism, functional improvement after stem cell therapy has been reported [36, 60, 61]. Moreover, the beneficial effect has been shown to be dose and time-dependent and certain amount of cells is required to observe beneficial results [62-64]. This underscores the importance of the efficiency of cell delivery. The amount of stem cells delivered and retained in the infarct site were very limited when the cells are administrated systematically [39]. Whereas direct injection into the infracted

myocardium or through coronary system provides more efficient ways to deliver the cells while these invasive procedures increase the risk of mortality.

Our group has reported a unique strategy to efficiently direct and distribute a large amount of stem cells using a bispecific antibody (BiAb) targeted to the damaged myocardium[40, 41], also in previous chapter. This observation was also reported in mice from other groups[43]. The BiAb was engineered by chemical conjugation of a CD45 monoclonal antibody (mAb) recognizing an antigen found in purified human CD34+ cells and a myosin light chain (MLC) mAb recognizing a cardiac-specific antigen expressed in injured myocardium. As a cytosolic protein in cardiomyocytes, MLC will be exposed to intravascular anti-MLC only when cell membrane is no longer intact during myocardial injury, thus the CD45 X MLC BiAb armed cells can be anchored and uniformly distributed in the damaged myocardium. Echocardiography showed this targeted delivery significantly preserved myocardial function 5 weeks after injury compared to unarmed CD34+ cells.

To further explore the advantages of BiAb targeting delivery, we have conducted a comparison study of direct injection of CD34+ cells to the injured myocardium guided by high-resolution echocardiography and BiAb targeted CD34+ cells. We observed that BiAb-homed HSCs preserve cardiac function comparable to if not better than direct injection of HSCs in MI.

6.2 Methods

6.2.1 Rat acute MI model

Thirty immunodeficient nude rats received 25 minutes occlusion of left anterior descending port of left coronary artery and then reperfused under anesthesia as chapter 2.

6.2.2 Arming of human CD34+ cells

Human CD34+ cells were recovered and reconstituted to 16million cells/ml and armed with CD45 x MLC BiAb for 15 minutes at 0.5μg/M such that the BiAb concentration was 8μg/ml and the arming efficiency was above 90% same as in chapter 3.

6.2.3 Administration of CD34+ cells

Two days after myocardial injury, 30 rats were grouped based on fraction shortening (in Echocardiography) as three groups: direct injection of 2M unarmed CD34+ cells, intravenously injection of 2M CD45 X MLC armed CD34+ cells, and intravenously injection of PBS as control. The details of administration methods were in Chapter 2.

6.2.4 Echocardiography

Transthoracic echocardiography was performed under anesthesia and details in chapter 2. Cardiac function was measured before, 10-12 days after, 5weeks after, and 3months after cell injection.

6.2.5 Histology

Sixteen weeks after infarction, the rats were euthanized and the hearts were immediately excised and fresh-frozen. The hearts were then sectioned into 10-μm slices throughout the infracted region and the representative slices were stained with Masson's trichrome stain for morphometric analysis. The infarct size is calculated as the infarct area percentage of left ventricle area (details in Chapter 2).

Six sections equally distributed through the infarct area were stained with mouse IgG1 anti-humanleukocyte antigen (HLA) class I (BD Pharmingen) to detect the CD34+ cells. Angiogenesis in the infarct was examined by immunohitochemical staining of CD31 (mouse IgG1 anti-CD31; BD Pharmingen 550300) and α-smooth muscle actin (mouse IgG2a anti-α smooth muscle actin; Sigma-Aldrich A2547) to detect capillaries and arterioles respectively. The staining assay was then finished with mouse-on-rat polymer kit (Biocare MRT511). Capillaries were identified as a single layer of CD31-positve cells and capillary density was obtained from five high-power fields in the infarct region per slide and averaged in the slides spanned the entire infarct. Arterioles were identified as a positive staining of α-smooth muscle actin with a lumen structure of a diameter between 10 and 100μm. Arterioles density was calculated as the average number of arterioles in the total infarct area from six representative slides.

6.2.6 Statistics

Based on fractional shortening 1 day after MI, the 30 rats were blocked as 6 barely damaged (35%<FS<45%), 18 damaged (25%<FS<35%), 6 severely damaged (FS<25%) .

Every group (IV armed, IM unarmed and PBS) consisted of the random selection of 2 animals from the barely damaged, 6 from the damaged, and 2 from the severely damaged. ANOVA was carried out and the p-value was reported using an unpaired 2-tail t-test.

6.3 Results

6.3.1 BiAb armed CD34+ cells preserve heart function comparable to direct injection

The PBS control group showed the typical negative remodeling following a MI. There was deterioration of left ventricle (LV) function, dilation of LV, and LV free wall thinning. In contrast, the groups treated with CD34+ cells demonstrated improved LV function, and attenuated wall thinning. As early as 2 weeks, fractional shortening (FS) in the both BiAb armed ($p=0.017$) and direct injection groups ($p=0.002$) increased significantly compared to the control group. This significant improvement was maintained for 5 weeks for both the BiAb armed group ($p=0.001$) and for direct injection group ($p=0.021$); while at 3 months, only the BiAb armed group ($p=0.0024$) was significantly better than the control group. This shift was partially due to the rat that died at 8 weeks with poor cardiac function in the control group rather than a big change in the direct injection group (figure 6.1a). Dilation of LV was attenuated in the treatment groups where the systolic LV dimension anterior wall thickness in BiAb armed group was significantly ($p=0.0129$) less than that in the group and that in direct injection was barely significant ($p=0.0520$) at week 5 and the difference is less obvious in month 3 due to the loss of rat in control group (figure 6.1b). In both systole and diastole, LV wall

thinning was retarded in the treatment groups and more significant in BiAb armed group ($p<0.05$) than in direct injection group ($p<0.1$) compared to the control group (figure 6.1 c d). All the echocardiography data were summarized in table 6.1 and represented as mean ± standard deviation.

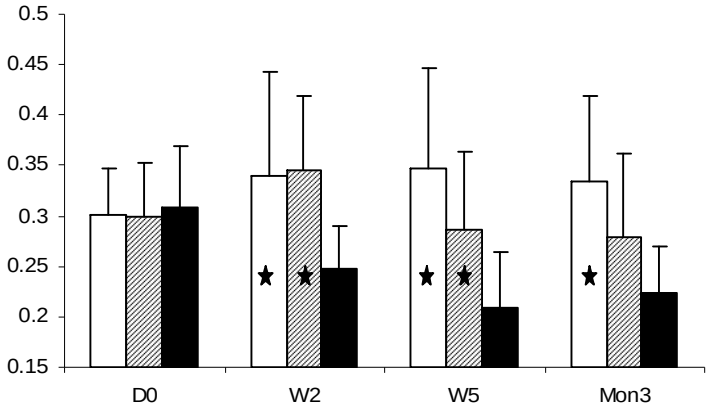

(a) Fraction Shortening

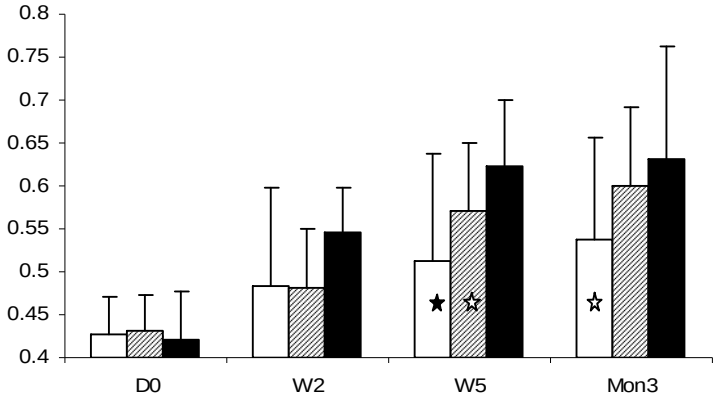

(b) Dimension in Systole

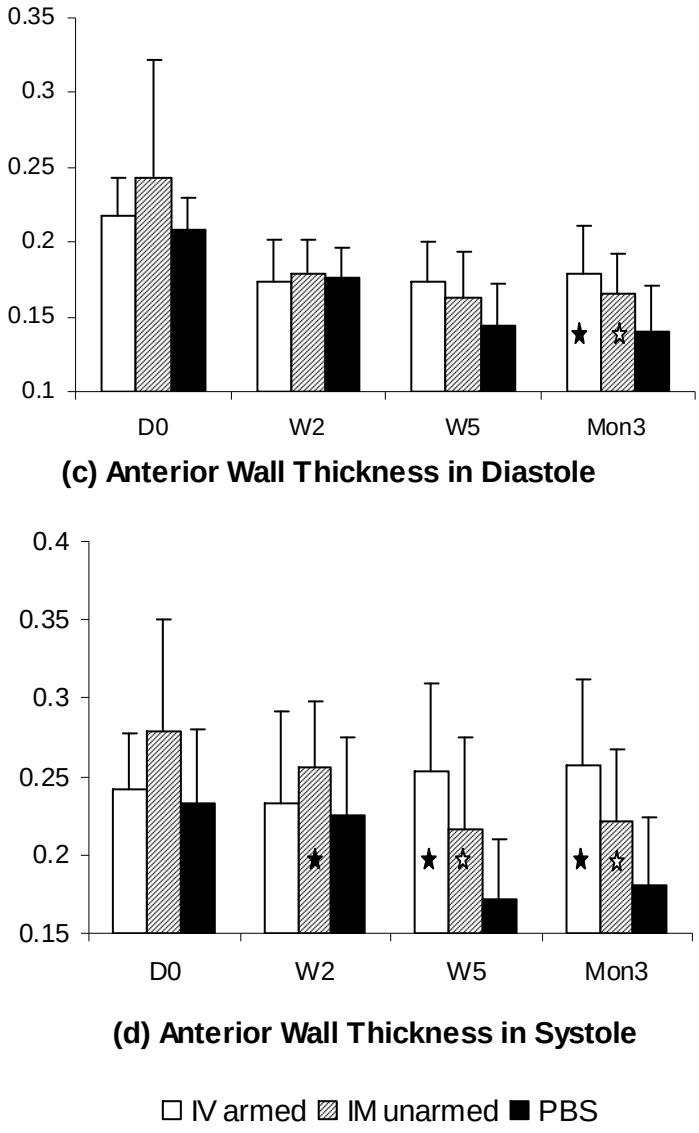

Figure 6.1 Echocardiography data show functional improvement in treatment groups and the group treated with armed cells intravenously (IV armed) shows similar improvement as the group treated with direct injection cells into myocardium (IM direct) at different time points after cell injection (D0 is before treatment baseline). All the data are represented as mean + standard deviation, solid star stands for statistically significant ($p<0.05$), hollow star stands for barely significant ($0.05<p<0.1$). Data were represented as mean + standard deviation.

Table 6.1 Echocardiography data.

	Baseline (D0) n=10	Week 2 n=10	Week 5 n=10	Month 3 n=10
FS (%)				
IV armed	30.10±4.68	34.02±10.33	34.69±10.04	33.48±8.48
IM unarmed	29.91±5.35	34.54±7.41	28.54±7.78	27.83±8.30
PBS control	30.77±6.15	24.70±4.36	20.97±5.46	22.39±4.63
LV Dimension in systole (mm)				
IV armed	0.427±0.042	0.4839±0.114	0.512±0.125	0.538±0.118
IM unarmed	0.432±0.0424	0.481±0.07	0.571±0.08	0.601±0.09
PBS control	0.232±0.05	0.545±0.052	0.623±0.08	0.631±0.132
LV wall thickness in systole (mm)				
IV armed	0.242±0.036	0.232±0.059	0.253±0.056	0.257±0.056
IM unarmed	0.279±0.071	0.255±0.042	0.216±0.059	0.222±0.046
PBS control	0.232±0.048	0.226±0.049	0.172±0.038	0.180±0.044
LV wall thick ness in diastole (mm)				
IV armed	0.218±0.25	0.173±0.029	0.173±0.027	0.178±0.032
IM unarmed	0.242±0.79	0.179±0.022	0.162±0.032	0.165±0.027
PBS control	0.208±0.022	0.176±0.020	0.143±0.028	0.139±0.032

6.3.2 BiAb homed CD34+ cells reduces infarct size comparable to direct injection

Infarct size, as the percentage of infarct area to LV area, showed similar trend (figure 6.2) as echocardiography. The BiAb armed group had similar infact size (31.12±7.7%, p=0.000604) to direct injection group (31.51±5.9%, p=0.000274); and both were significantly smaller than PBS control group (48.04±9.2%).

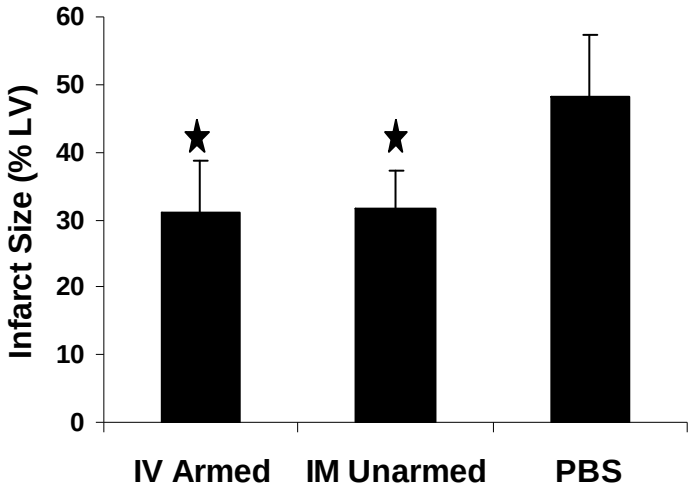

Figure 6.2 Infarct size. The IV injection of armed CD34+ cells resulted in similar infarct size; both reduced infarct size significantly ($p<0.05$) compared to injection of PBS. Data were represented as mean + standard deviation.

Although two treatment groups had similar infarct size, the scar in the IV armed group (figure 6.3 b) was more sparse than that in the IM unarmed group (figure 6.3 a). The infarct sizes were 28.49% and 33.19% respectively. Transmural infarcts were more often in PBS control group as in figure 6.3c with an infarct size of 43.44%.

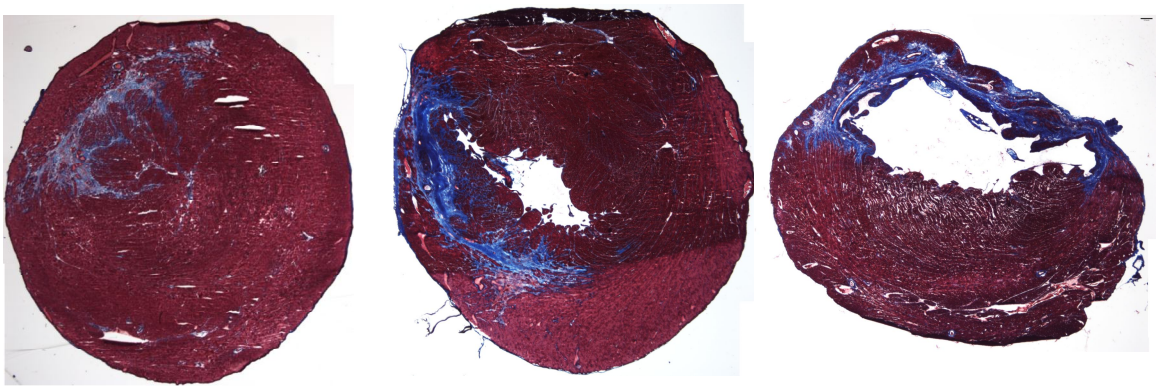

(a) (b) (c)

Figure 6.3 Masson's trichrome staining of three slides with infarct size close to the average infarct size in the group from IV armed group (a) (28.49%), direct injection group (b) (33.19%) and PBS control (c) (43.44%). The pattern of infarct was denser in HSC direction injection group than in IV armed group and more transmural infarcts were observed in PBS control.

6.3.3 BiAb targeted CD34+ cells promote angiogenesis and uniform neovascularization

Angiogenesis was assessed as capillary density and arteriole density. CD31 staining for capillaries and α-smooth muscle actin staining for arterioles revealed that increased average capillary and arteriole density in the CD34+ treated groups (table 2, mean±standard deviation).

Table 2 Angiogenesis data

	Capillary density (#/mm^2)	Arterioles density (#/mm^2)
IV armed	277.9±43.0	10.26±3.07
IM unarmed	259.1±37.8	10.04±2.44
PBS control	218.7±28.9	7.72±1.65

The average arteriole densities (figure 6.4) and capillary density (figure 6.5) in BiAb armed group and direct injection group were higher than the PBS group.

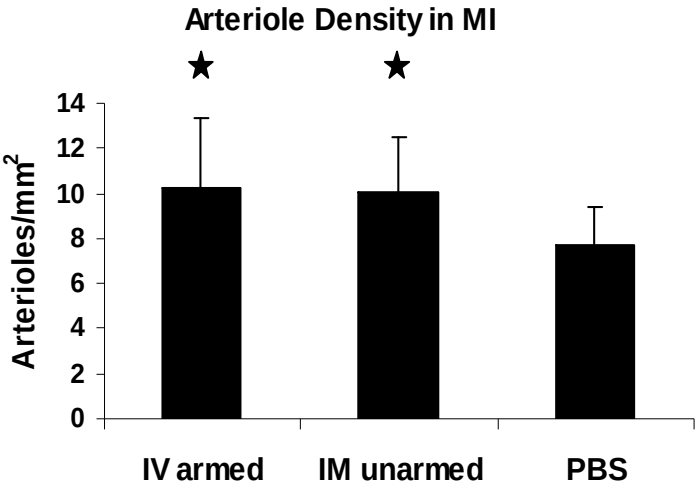

Figure 6.4 Arteriole density. The IV injection of armed CD34+ cells and direction injection of CD34+ cells increase the arteriole density significantly ($p<0.05$) compared to injection of PBS. Data were represented as mean + standard deviation.

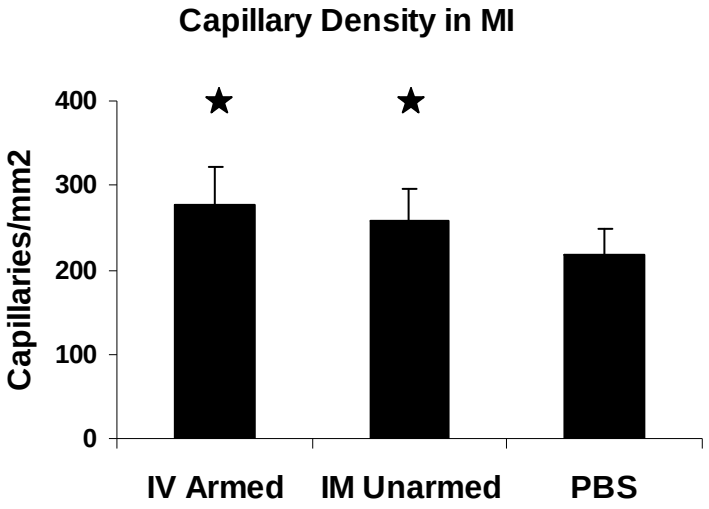

Figure 6.5 Capillary Density. The IV injection of armed CD34+ cells and direction injection of CD34+ cells increase the capillary density significantly ($p<0.05$) compared to injection of PBS. Data were represented as mean + standard deviation.

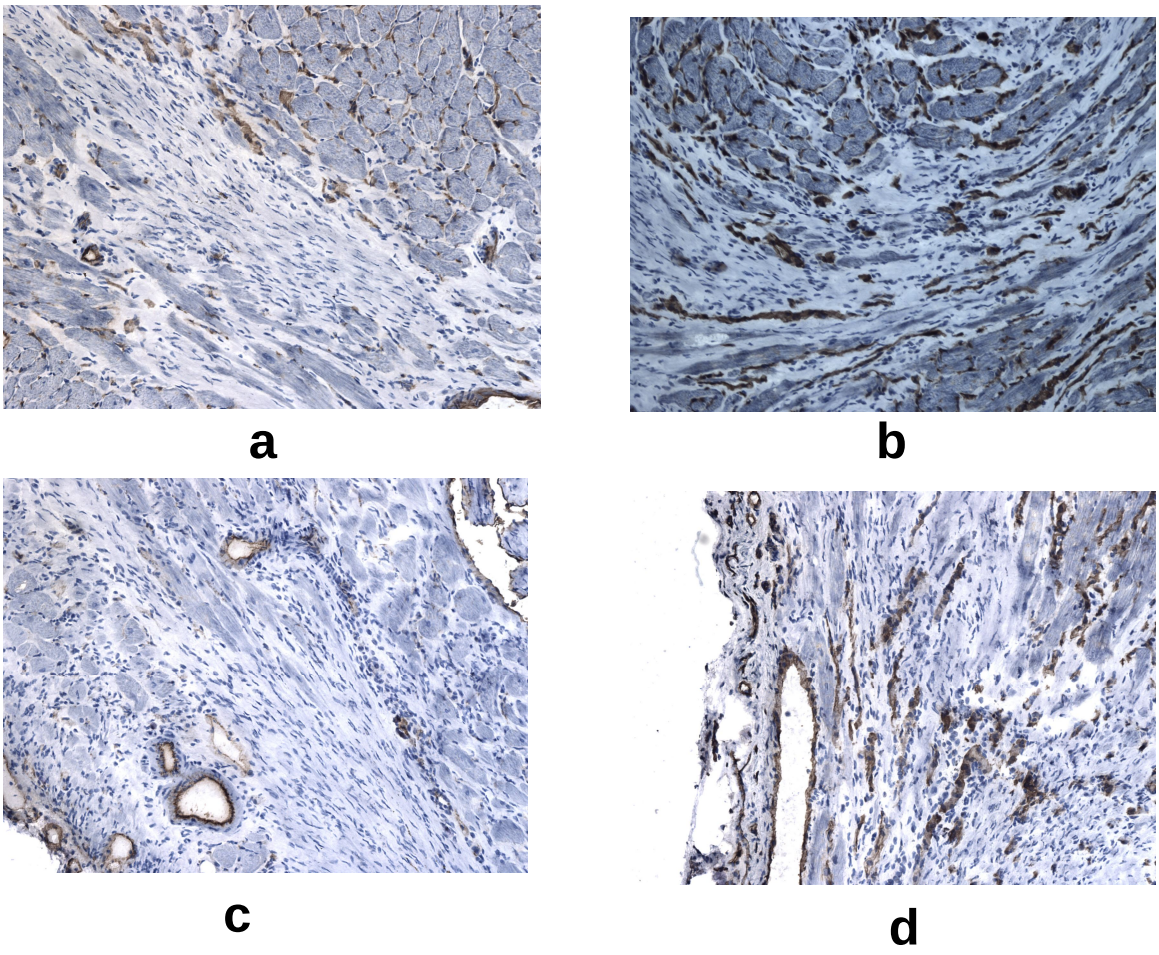

Figure 6.6 Staining of capillary at the border of MI in PBS (a), BiAb (b) and direct injection group (c, d). Capillary density in direction group varies greatly in different sites and it is as sparse as PBS group (c) or as dense as BiAb group (d).

Representative pictures of CD31 staining were selected (figure 6.6) to demonstrate that there are fewer capillaries in the infarct region especially at the border of the infarct in the PBS group (figure 6.6a) than in the BiAb (figure 6.6b) targeted group. The capillary density in the direct injection group had a big variance depending on the location within the MI. Capillary density could be as sparse as in the PBS group (figure 6.6c) and as dense as or denser than the BiAb targeted group (figure 6.6d) in the same animal. This might be explained as the proximity to the injection site.

6.4 Discussion

This study demonstrated the long term effectiveness of antibody targeting technology in stem cell therapy for cardiac repair. Human HSCs armed with BiAb at predetermined optimal concentration exhibited comparable beneficial effects in treating MI as the commonly used direct injection of the same amount of human HSCs. After 16 weeks, no human marker could be detected by histological analysis (data not shown). The cardiac contraction, wall thickness, LV dilation, infarct size, and neovascularization as increased capillary and arteriole density were significantly better in the BiAb armed group and direct injection group than those in the control group. The beneficial effects in the BiAb armed group were as good as or even better, although not significant, than the direct injection group. Combined with previous reports demonstrating BiAb targeted HSC improve LV function [41, 43], we conclude that antibody targeting approach provides a non-invasive, efficient, and effective delivery method for cardiac stem cell therapy.

The BiAb technology provided a way to bring in a man-made myocardial injury specific molecule to any therapeutical agent. Despite the potential loss of efficiency as MLC is released into circulation upon injury, we observed a remarkable amount of HSCs homed to the injured myocardium (chapter 5). Moreover, the improvements were about the same in both treatments and we observed more sparse MI and more uniform neovascularation in the BiAb armed group than the direct injection group. This might be explained as HSCs were brought to the MI through the circulation and thus more in the border of MI where part of vasculature is still functional and provides more favorable milieu for HSCs than the center of MI. Whereas the injection site in the approach of direct injection is less under control and partly response for the inconsistence of the other studies using direct injection. The difference in the HSCs distribution in two treatments may explain the similar improvement while possible different amount HSCs in two treatments. A further study to determine the homing efficiency and compare the improvement of direct injection and BiAb homed which yield the same amount cells in MI will help to elucidate the effect of uniform distribution of therapeutical cells.

Unlike the previous study[41] ended at 5 weeks after HSCs injection and some HSCs persisted at the end of study, we did not observe any HSCs 16 weeks after injection while we observed significantly increased neovascularization. This agrees with other clinical studies and the beneficial effect may be explained by paracrine effect of HSCs. The secretion of HSCs might have modified the milieu in the MI, induced angiogenesis, helped the survival of cardiomyocytes, and further retarded the negative remodeling

process. The transplanted HSCs may undergo apoptosis or removed in long run, but the beneficial effect is sustained for at least 3 months.

In summary, this study further proved the effectiveness and uniqueness of antibody targeting technology in cardiac stem cell therapies. It also brings a new way to deliver stem cells uniformly to MI and enhance the beneficial results.

Chapter 7:

Effect of BiAb armed HSCs on electrophysiology (submitted)

7.1 Introduction

MI causes the loss of contractive components of the heart causing mechanical dysfunction leading to heart failure. However, more than half of heart failure patients die of sudden apparent arrhythmias. During the processes of remodeling after MI, such as, necrosis and apoptosis of cardiomyocytes, infiltration of fibroblasts, slippage of survival cells, and formation of fibrotic tissues, not only contractility of the heart is affected but also conductivity. The heterogeneity in conduction provides a substrate for arrhythmias and therefore it is also important to study whether or not a treatment is proarrhythmia.

This antiarrhythmia or non-proarrhythmia criterion is also applied to cardiac cell therapies besides the other criteria, such as cell source, cell survival after transplantation, and contractility improvement. Skeletal myoblasts were extensively studied in the early exploration of cardiac cell therapies[18, 19] because 1) they can be isolated from a muscle biopsy and subsequently expanded; 2) they are not so sensitive to oxygen supply as cardiomyocyte so that they can survive in MI; 3) they are naturally contractive. Despite all the advantages, skeletal myoblasts do not form gap junctions and thus it is unlikely that they contract synchronously with the surrounding cardiomyocytes [30].

Additionally, skeletal myoblasts can further differentiate into fast-beating myotubes and electrical instability has been seen in some patients transplanted with skeletal myoblasts in phase I and II clinical trials [29, 65]. In other words, skeletal myoblasts might be proarrhythmia after transplantation and their use in cardiac cell therapy is still under considerations.

Whether or not a cardiac cell treatment is proarrhythmia does depend on not only the characteristics of the therapeutic cell itself but also the possible heterogeneity in action potential duration (APD) introduced by transplantation of non-cardiac cell, or even by uneven sympathetic activities in MI due to nerve sprouting around the site of cell injection.

Hematopoietic stem cells (HSCs) improve heart function after MI mainly by paracrine effects and angiogenesis in MI border zone during remodeling process which, in turn, help the survival of native cardiomyocytes and further reduces the extension of scar formation. Although HSCs have not been associated with cardiac arrhythmia, few studies have explored the effect of HSCs on electrophysiological properties of the heart. Here we conducted a study which attempts to explore the effect of HSCs on ventricular tachycardia (VT) inducibility, conduction velocity and APD.

7.2 Methods

7.2.1 Rat acute MI model

Fifteen immunodeficient nude rats received 25 minutes occlusion of left anterior descending port of left coronary artery and then reperfused under anesthesia as chapter 2.

7.2.2 Arming of human CD34+ cells

Human CD34+ cells (Cambrex, now Lonza) were recovered and reconstituted to 16million cells/ml and armed with CD45 x MLC BiAb at 0.5μg/M such that the BiAb concentration was 8 μg/ml and the arming efficiency was above 90% according to titration from chapter 3 (Chapter 3, figure 3.1). The cells were incubated with the BiAb for 15min at room temperature and then washed twice by spinned down and resuspended in PBS.

7.2.3 Administration of CD34+ cells

Two days after myocardial injury, 15 nude rats were grouped to three groups: direct injection of unarmed CD34+ cells, intravenously injection of CD45 X MLC armed CD34+ cells, and intravenously injection of PBS as control (chapter 2).

7.2.4 Echocardiography

Transthoracic echocardiography was performed under anesthesia and details in chapter 2. Cardiac function was measured before, 5weeks after administration of the cells.

7.2.5 Optical Mapping

Optical Mapping was performed five weeks after cell treatment. All the rats receive 500U heparin intraperitoneally 15 minutes before anesthetized with pentobarbital

(50mg/kg). Then the heart was rapidly harvested, cannulated through the aorta and perfused at 6ml/min with 37°C modified-Tyrode solution with a content of 121.7mM NaCl, 25.0mM NaHCO3, 4.81mM KCl, 2.74mM MgSO4, 2.0mM CaCl2, and 5.0mM dextrose. The modified-Tyrode solution was bubbled with 95% O_2 and 5% CO_2. The heart was then transferred to a custom-built optical mapping chamber and 15mmol/L 2,3-butanedione monoxime was added in modified-Tyrode solution as excitation-contraction uncoupler.

Light from a 1000W tungsten-halogen lamp (Spectra-Physics,Model 66921) via fiberoptic cables was directed onto the field of view for illumination . Care was taken to illuminate the imaging surface homogenously. Optical mapping images of 100x100 pixels were obtained with an excitation filter of 530nm and emission long-pass filter with cutoff of 630nm. Images were acquired by an ultra fast imaging system MICAM ULTIMA(Scimedia) at 1000Hz.

7.2.6 Pacing protocol

The perfused hearts were first applied with ventricular epicardial bipolar pacing for 20 cycles at pacing cycle length (PCL) 200, 180, 150, 130, and then decreased by 10ms until no capture and the last second data were recorded for each PCL. Then a S1-S2 protocl was applied with a basic pacing cycle length of 200ms for 20 cycles and S2 from 150, 130, 120ms and then decreased by 10ms until effective refractory period (ERP). Burst pacing was applied from 100ms to 60ms by a decrement of 2ms to induce ventricular arrythmias. Non-sustained VT was defined as 2 or more ventricular beats but lasting less

than 30 seconds. Sustained VT was defined as sustained ventricular tachycardia > 30 seconds or ventricular fibrillation (VF).

7.2.7 Data analysis

All the programs were written in free software R version 2.7.2 (ISBN 3-900051-07-0). Quantitative analysis was performed by identifying activation of each optical action potential as the maximum dF/dt. Isochronal activation maps, conduction velocity (CV), velocity vectors[66], and rise time (time between takeoff and peak of the action potential) were analyzed[67, 68]. Action potential duration was determined as APD50 and APD80 (duration from the activation to the point at which the amplitude has recovered to 50% and 80% of its maximum, respectively).

7.3 Results

7.3.1 Echocardiography

Due to the smaller sample size (n=5), there was no statistical significant difference between groups. However, echocardiography showed similar trend as the study with larger sample size (n=10) in chapter 6 and cardiac function was worse in the control group but well preserved in the treated groups without statistical significance. Fractional shortening was charted in figure 7.1 to demonstrate such a trend.

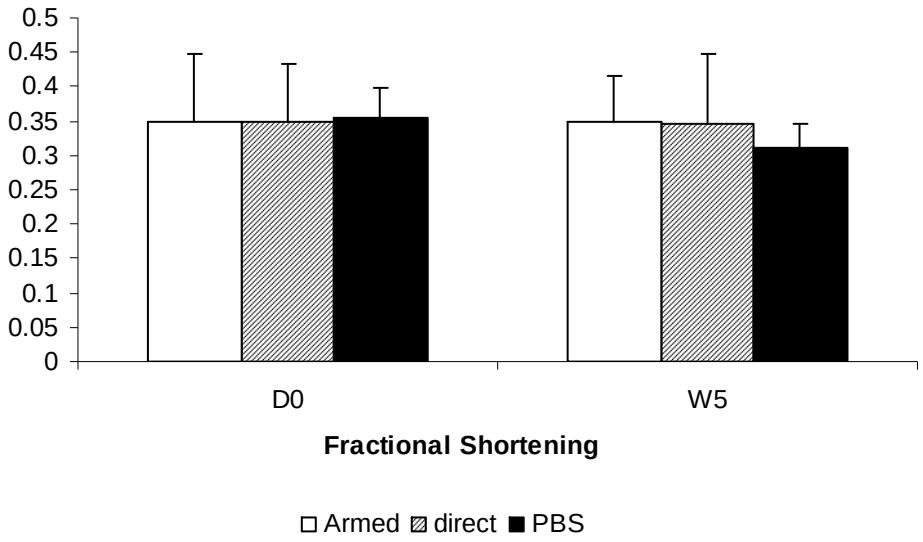

Figure 7.1 Echocardiography data show functional improvement in treatment groups and the group treated with armed cells intravenously (IV armed) shows similar improvement as the group treated with direct injection cells into myocardium (IM direct). Although there was no statistical significance due to sample size, the results showed similar trend as larger sample size studies. All the data are represented as mean + standard deviation.

7.3.2 Ventricular tachycardia inducibility

In PBS control group (PBS), one out of five had sustained VT and two had non-sustained VT (60%). Whereas in the group treated with direct injection cells into myocardium (IM direct), two out of five had non-sustained VT (40%); and one out of five had non-sustained VT in the group treated with armed cells intravenously (IV armed) (20%). If 60% was a good estimate of VT inducibility in MI rats without HSC treatment, then the VT inducibity in IV armed group was less than control with p=0.08704.

7.3.3 Electrophysiological alteration in MI

The perfused hearts were paced 20 cycles at different pacing cycle length (PCL) of 200ms, 180ms, 150ms, 130ms, and then decreased by 10ms until no capture, no capture PCL ranged from 60 to 110ms. Conduction velocity, APD80, APD50, APD30, and rise time, time between takeoff and peak of the action potential,were obtained at all captured PCL at all recordings sites for each animal. Whether a recording site was in MI or normal tissue was determined by the amplitude of the signal at that site and verified with unfiltered image.

Conduction velocity vector were calculated [66] and average magnitude of conduction velocity was obtain in MI and normal tissue respectively. Averaged conduction velocity in all 15 hearts was about 20% slower in MI than normal tissue. The difference was more significant at long PCL as $p<0.01$ at PCL from 200 to 90ms and $p<0.05$ at 80 and 70ms. Conduction velocity decreased when PCL decreased and this was more obvious with short PCLs .

Action potential duration (APD) were computed as time from takeoff to 80%, 50%, or 30% of recovery and also averaged in MI and normal in all 15 hearts. APD80 in MI was significantly ($p<0.05$) longer than normal tissue at PCL 200, 180, 150ms; APD50 in MI was significantly longer than normal tissue at PCL 200, 180, 150, 130, 120ms; and APD30 in MI was significantly longer than normal tissue at PCL 200, 180, 150, 130, 120, 110, 100ms.

Average rise time in all 15 hearts was longer in MI than normal tissue at all PCLs from 200 to 70ms. Bigger standard deviation at shorter PCLs because of less capture at shorter PCLs (n=15 for PCL=200-110ms; n=14 for PCL=100ms; n=12 for PCL=90ms; n=8 for PCL=80ms; n=2 for PCL=70ms).

7.3.4 Different CV in MI in different groups

Conduction velocity in normal tissue had no significant difference in all three groups However, more difference in CV was observed in MI among groups (figure 7.2.a). Conduction velocity in MI was significantly larger in IV armed group than PBS group at PCL 110ms, 100ms, and 90ms. There was no significant difference in CV between IM unarmed group and PBS group because the large variance within IM unarmed group and small number in each group.

7.3.5 Treatment effect on APD

Within normal tissue, there is no significant difference in averaged APD80, APD50, and APD30 among all the three groups (data not shown).

Although both IV armed and IM unarmed groups had shorter means of APD80, APD50, APD30 than PBS control group in MI (data not shown), only APD50 at PCL=200ms in IV armed group was significantly shorter than that in PBS control group (figure 7.2.b)

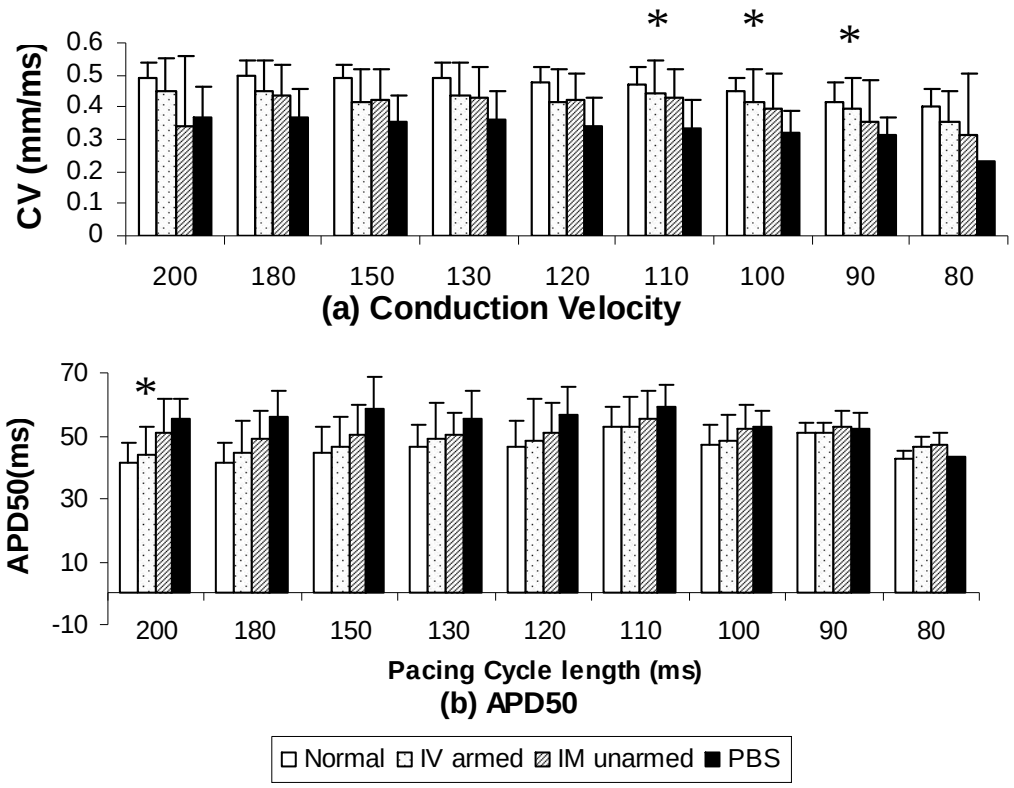

Figure 7.2 Electrophysiological properties in MI. (a) Conduction velocity in MI was significantly larger in IV armed group than PBS control group at PCL 110ms, 100ms, and 90ms. (b) APD50 in MI was significantly shorter in IV armed group than PBS control group at PCL 200ms. Averaged conduction velocity and APD50 in normal tissue in all 15 hearts were plotted for reference. Data represented as mean + standard deviation. *: $p<0.05$ comparing with PBS control.

7.4 Discussion

This study demonstrated that 1) electrophysiological properties were significantly changed in MI region; 2) HSCs were not arrhythmogenic; and 3) CD45 x MLC armed HSCs group showed significantly better electrophysiological properties than the control

group. Within the MI region, conduction velocity was more than 20% slower; APD was 10% longer especially with longer pacing cycle length; and rise time was 20% longer than those in normal tissue respectively.

Ventricular tachycardia inducibility did not increase in the animals receiving HSCs. In fact, HSCs even decreased ventricular irritability in the IV armed group ($p=0.08704$) although not significant. HSC treatment did not affect conduction velocity in normal tissue but in MI especially at short pacing cycle length. Conduction velocity in MI was significantly faster in the IV armed group than control group at pacing cycle length 110ms, 100ms and 90 ms therefore the averaged CV relatively closer to CV in normal tissue. Action potential duration in MI was significantly shorter in IV armed group than in control group at pacing cycle length 200ms. These findings proved that treating MI with HSCs was not proarrhythmic and agreed with other people's report [69].

These beneficial effects in IV armed HSCs group was more of a secondary effect from prevention of negative remodeling, improvement in blood supply in border zone, and preserved cardiac function rather than a direct effect of HSCs as our previous observations and other people's studies showed low transdifferentation rate of the transplanted cells.

It is interesting to notice that IV armed HSCs perform better than direct injection of unarmed HSCs. The IV armed group was significantly better than the control group in some of the electrophysiological properties while the beneficial effect in IM unarmed

group was not significant. The difference was more from the large variance in the IM unarmed group and this challenged our assumption that the variance in each group was the same after treatment. Whether or not the larger variance in IM unarmed group was true needs more study to find out. However the difference in variance hinted that the homing method provided a more uniform repair of the damaged tissue through circulation and brings the armed cells in a microenvironment close to blood supply; therefore, homed cells have a better chance to survive. In contrast, direct injection delivered the cells in a relative random way which depends on the person performed the procedure. Cells injected at border zone would be expected more effective than cells injected in the center of MI where the vasculature was more severely damaged and this may lead to a less stable outcome than the homing method. We did observe larger variability in all the measurement qualitatively. However, with a small sample as we have, we need further studies to verify this.

Chapter 8:

Time series analysis of optical mapping data in MI rat

8.1 Introduction

Analysis of optical mapping data is time-consuming and subject to the analyzer's experience and personal preference. To determine activation time at one location, the traditional approach is to select the activation time at which dF/dt is maximum of one arbitrary beat (method in chapter 7). This approach is accepted in the community and performs well when the signal noise ratio (SNR) is good enough. However, the signal amplitude is much smaller in MI due to the cardiomyocytes death in MI and SNR is too small to make a meaningful analysis. Therefore, signals from the center of MI, whose signal amplitude is lower than a certain threshold, are discarded. In MI region, the signal is contaminated by noise and hard to decide activation time. Consequently, the conduction velocity is hard to determine as it is calculated as the ratio of the distance and the difference in time between two recording spots. In order to assess the electrophysiological effects of stem cell therapy for MI, it is indispensable to obtain information from MI region.

Here I proposed two approaches based time series analysis theories to explore optical mapping data in MI rat. 1) Obtain isochronal map including MI region using the cross-correlation function (CCF) during monomorphic VT. CCF gives the similarity between two time series at different lag time. CCF is maximized at the lag with largest similarity

and CCF of one signal to itself is maximized at lag 0. During monomorphic VT, it is reasonable to assume that local signal is periodic and the lag time at maximum CCF is a good approximate of the difference between activation times [70]. 2) Complex demodulates monomorphic VT. Complex demodulation is a spectral estimation method well tested in the geophysical field [71] and it combines nonlinear regression and complex demodulation and attempts to minimize the error in each potential interesting frequency based on spectral estimation.

The optical mapping signal was a spatiotemporal data set recorded by a CCD camera (MiCAM02, SciMedia). This spatiotemporal data set during induced ventricular tachycardia (VT) is composed of frames of 40 x 28 images and time interval between frames is 1.3ms. All codes were written in R.

8.2 Time domain analysis

CCF was calculated between a selected "good" (high SNR) signal (here, row 14, column 15, labeled as (14, 15), same in the follow) and all other signals as equation 8.1.

$$\rho_{x1,x2}(s,t) = \frac{\gamma_{x1,x2}(s,t)}{\sqrt{\gamma_{x1}(s,s)\gamma_{x2}(t,t)}} \qquad \text{(Equation 8.1)}$$
$$\gamma_{x1,x2}(s,t) = E[(x_{1s} - E(x_{1s}))(x_{2t} - E(x_{2t}))]$$

$x1$ and $x2$ were two signals from two different locations and there were 40x28=1120 signals in the data set. x_{1s} and x_{2t} were value of $x1$ and $x2$ at time s and t respectively, s, t were range from 1 to the length of data in time. E stood for expected value. Small portion of example signals and CCF are shown in monomorphic VT (figure

8.1) with high SNR in the left hand side signal (from location(16, 18)) and low SNR in the right hand side signal (from location (29,11)). In monomorphic VT, the signals are periodic which is also shown in CCF.

From the lag times with the largest CCF, the isochronal map was reconstructed (figure 8.3) in monomorphic VT. The isochronal map showed the conduction abnormality in the upper left and middle right parts of the heart, which correlated to the MI. The activation started from the top of the heart (base) and propagated down the bottom of the heart (apex). The activation was slowed at the abnormal conduction areas due to slower conduction in MI and move forward in the center of the heart until it encounters the activation propagated from the back of the heart (unable to see). These two wavefronts (one from the front in figure 8.3, one from the back) blocked each other due to refractory and divides to two new wavefronts travels left and right and then travel back up separately. This time the two upward wavefronts meets at the base of heart and a new cycle begins. There is a typical figure of "8" ("∞") shape wave form with the left clockwise one and the right counter clockwise one.

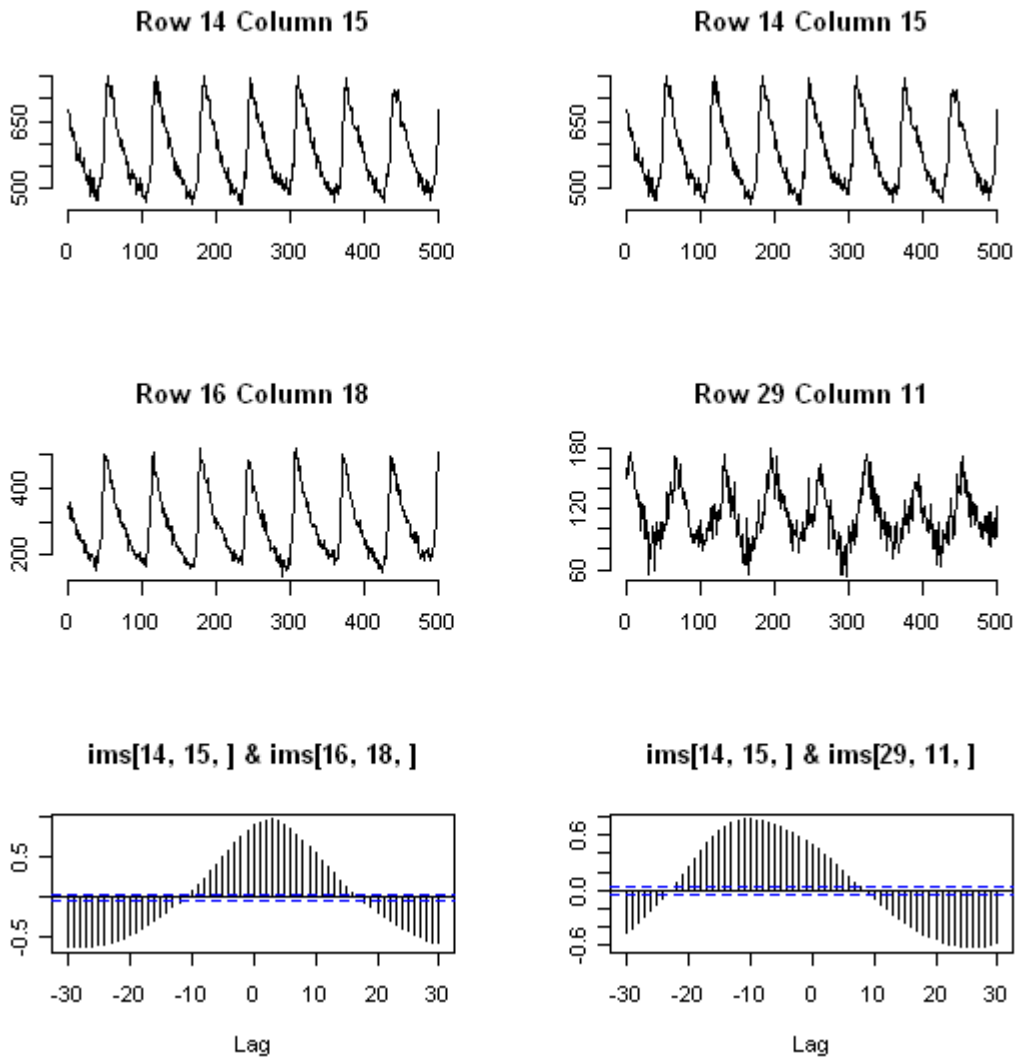

Figure 8.1 CCF in monomorphic VT signals. Reference signal was from row 14, column 15 (top panels). Two signals were from row 16, column 18 (left, middle) and row 29, column 11 (right, middle). CCFs were plotted in bottom panels respectively.

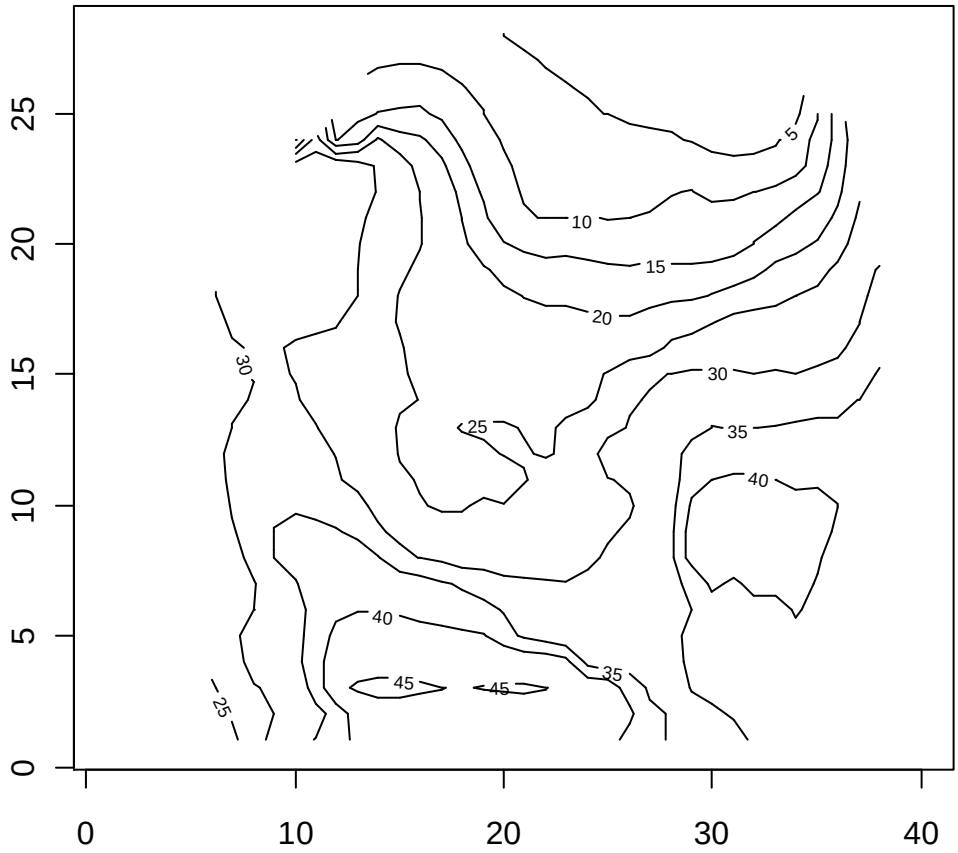

Figure 8.2 Isochronal map constructed from CCF

Although this CCF-lag method worked great with monomorphic VT, it did not perform well with polymorphic VT. This was because the main frequency changed not only from time to time but also from one spot to the other. In other words, signal from spot one switched from frequency f1 to frequency f2.

8.3 Complex demodulation analysis

Smoothed periodograms, the unbiased estimation of spectrum [70], were plotted in figure 8.3 and figure 8.4 for the two signals from locations (16, 18), (29, 11) respectively. It could be observed that estimated spectrum from (16, 18) was about 100 times larger than estimated spectrum from (29, 11) due to the difference in SNR.

Each peak or lobe in the spectrum stood for one frequency component in the signal and the area under each lobe was the energy associated with this frequency. The little bumps under certain threshold could be considered as noise and the blue bar at the right top corner was the threshold with 95% confidence interval of no significant difference from zero to eliminate noise. It would be ideal to reconstruct signal from the information given in smoothed periodogram. However, periodogram only gave energy (amplitude) at given frequency and there was no phase information included. Discrete Fourier transform (DFT) was although not an unbiased estimation of Fourier transform of the signal, it gave phase information. Complex demodulation utilized both information to reconstruct signal which minimize the difference in smoothed periodogram of recorded signal and reconstructed signal, in other words, nonlinear regression in frequency domain.

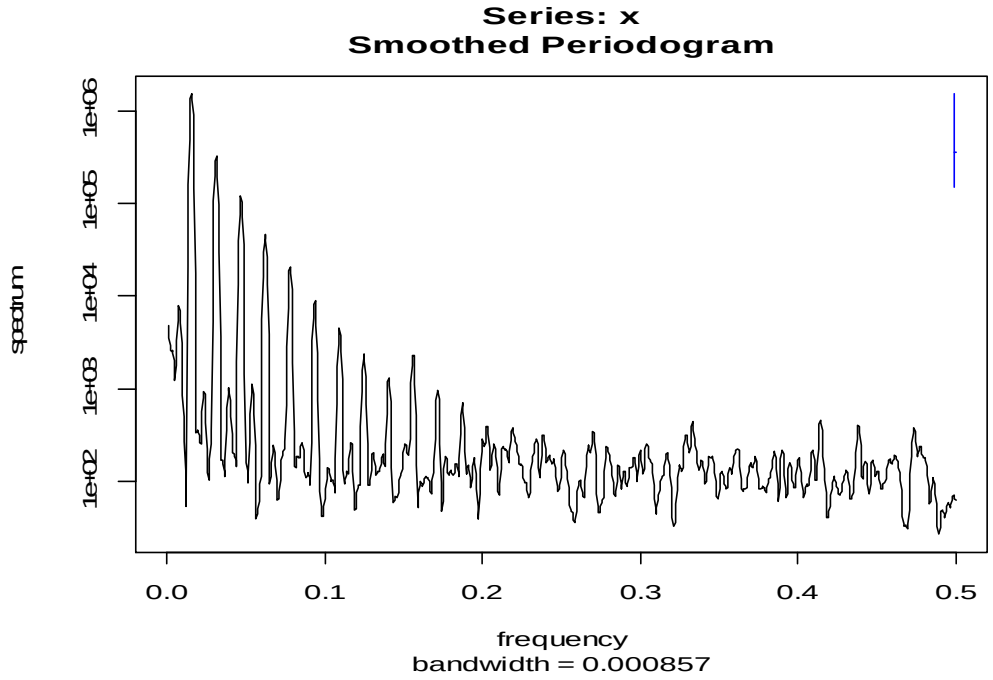

Figure 8.3 Estimated spectrum of signal from (16, 18) with large SNR

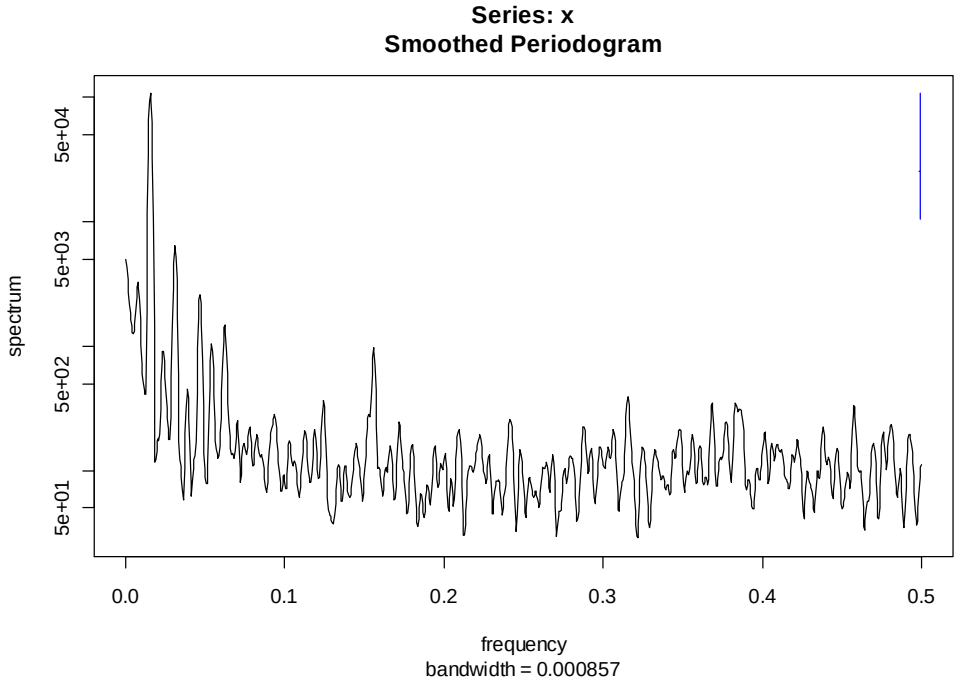

Figure 8.4 Estimated spectrum of signal from (29, 11) with small SNR

The parameters to be estimated were the amplitude, phase, and frequency of each lobe in smoothed periodogram. The initial value for the frequency can be determined from the smoothed periodogram while phase and amplitude were initialized as phase and amplitude at the initial frequency in DFT. Local minimization within the frequency range determined from smoothed periodogram reached by non-linear minimization using quasi-Newton method (function nlm() in R). In such way, it also decreased the error introduced by digitalization. Initial values and final estimates of signal (16, 18) were listed in table 8.1.

Table 8.1 Complex decomposition results for monomorphic VT

Initial Values			Estimates		
Frequency	Amplitude	Phase	Frequency	Amplitude	Phase
0.0078125	8427.3309335	-2.5994430	0.007811732	8427.331	-2.5994430
0.01.562500	120878.4	2.806549	0.015622014	120878.366	2.8065486
0.03125000	54854.65	0.3558304	0.031243859	54854.647	0.3558304
0.046875	32873.170486	-2.108755	0.046867332	32873.170	-2.1087550
0.062500	19855.764055	1.857977	0.062486981	19855.764	1.8579766
0.0781250	11706.0333727	-0.4713101	0.078107447	11706.033	-0.4713101
0.093750	7629.129629	-3.019792	0.093734753	7629.130	-3.0197916
0.1093750	4426.0430875	0.9381002	0.109345620	4426.043	0.9381002
0.125000	3117.772256	-1.694295	0.124993131	3117.772	-1.6942945
0.1557617	4813.0960000	-2.8447139	0.155840549	4813.096	-2.8447139

In order to demonstrate the effectiveness of complex demodulation, part of original signal (500 out of 2046), reconstruct data, and the residuals were plotted in figure 8.5 (from location (16,18)) and figure 8.6 (from location (29, 11)). The reconstructed signal reproduced the main features of the original signal and most importantly, the depolarization times were reconstructed well.

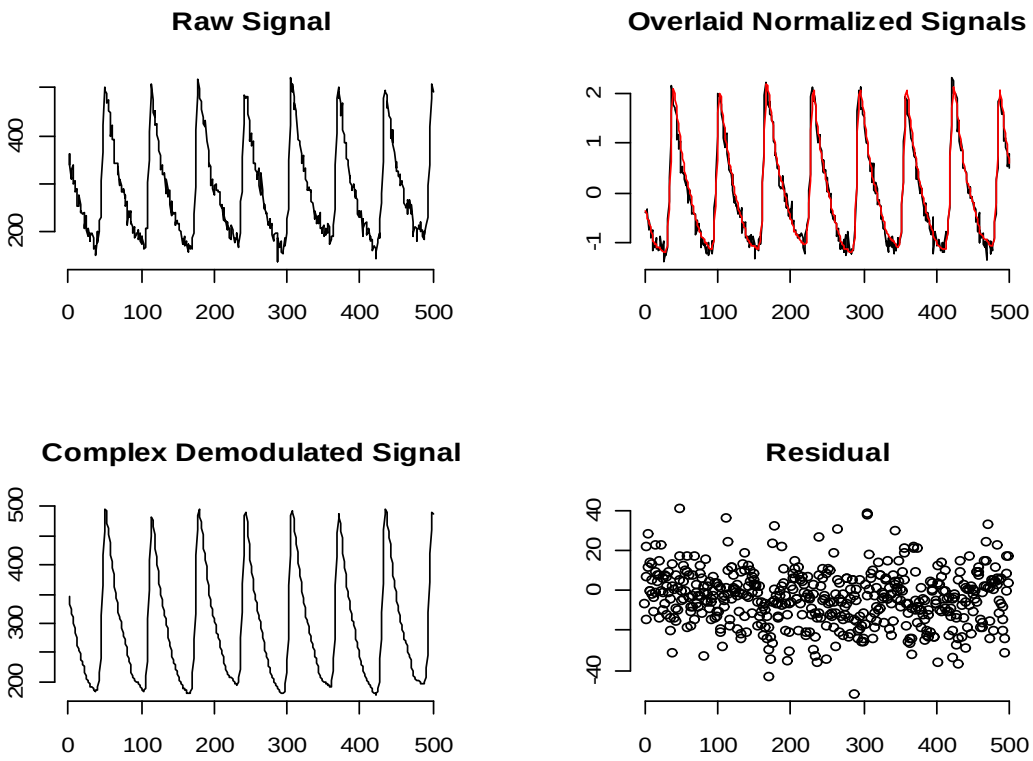

Figure 8.5 Complex demodulation results for signal from (16, 18). Top left panel: raw signal. Bottom left panel: reconstructed signal. Top right panel: raw signal (black) and reconstructed signal (red) overlaid after normalization. Bottom right panel: residual=raw signal – reconstructed signal.

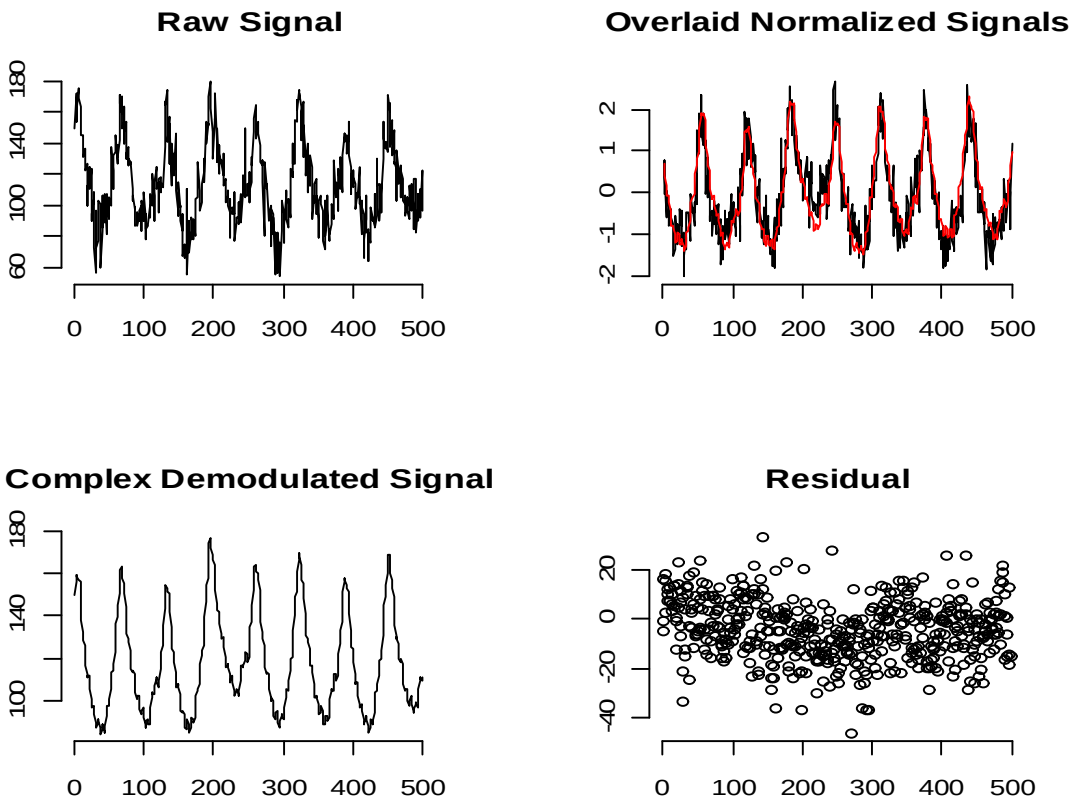

Figure 8.6 Complex demodulation results for signal from (29,11). Top left panel: raw signal. Bottom left panel: reconstructed signal. Top right panel: raw signal (black) and reconstructed signal (red) overlaid after normalization. Bottom right panel: residual=raw signal – reconstructed signal.

In order to further gauge the accuracy of complex demodulation, residual, defined as difference between raw signal and reconstructed signal, was further analyzed (figure 8.7 and 8.8). If complex demodulation reconstructed the optical mapping signal well, the residual should come from background noise such as thermo noise from CCD camera and random noise from outside circumstance during recording. The random noise should be stationary and pure random which means it was distributed invariant with respect to time.

With the large amount data, it is reasonable to assume the random noise was stationary Gaussian noise. The thermo noise would be expected to have similar structure as they are recorded by the same CCD and there would be an autoregression (AR) component because the thermo noise of CCD would propagate from one time to the time after that.

Normal quantile-quantile (Q-Q) plot, a graphical tool to diagnose the difference of data distribution and theoretical normal distribution for randomness (function qqnorm() in R), was plotted for the residual. More closely the Q-Q plot to a straight line, more random and close to normal distribution the residual is. An AR process of order p (AR(p), the current value only depends on the previous p values) can be characterized as partial autocorrelation function (PACF) cuts off at lag p and autocorrelation function (ACF) tail off (page 109 in [70]).

Analysis of residuals from signals with high SNR (from (16, 18), figure 8.7) and with low SNR (from (29, 11), figure 8.8) demonstrated similar results. 1) Normal Q-Q plots were very close to straight line and proved that the residual was normal distributed. 2) ACF tailed off in both cases and PACF cut off at 6 for signal from (16, 18) and at 7 for signal from (29, 11). The blue dashed lines in ACF and PACF indicated the 95% confidence interval of zero. This verified that the residual was AR process because thermo noise propagated along time. 3) The smoothed periodogram was close to spectrum of Gaussian noise except for the low frequency part.

A little tweak with this model was the low frequency component in the spectrum of the residual. This came from the low frequency fluctuation of the amplitude of the activations which was included in the model as the low frequency fluctuation of amplitude would not affect the accuracy of activation time.

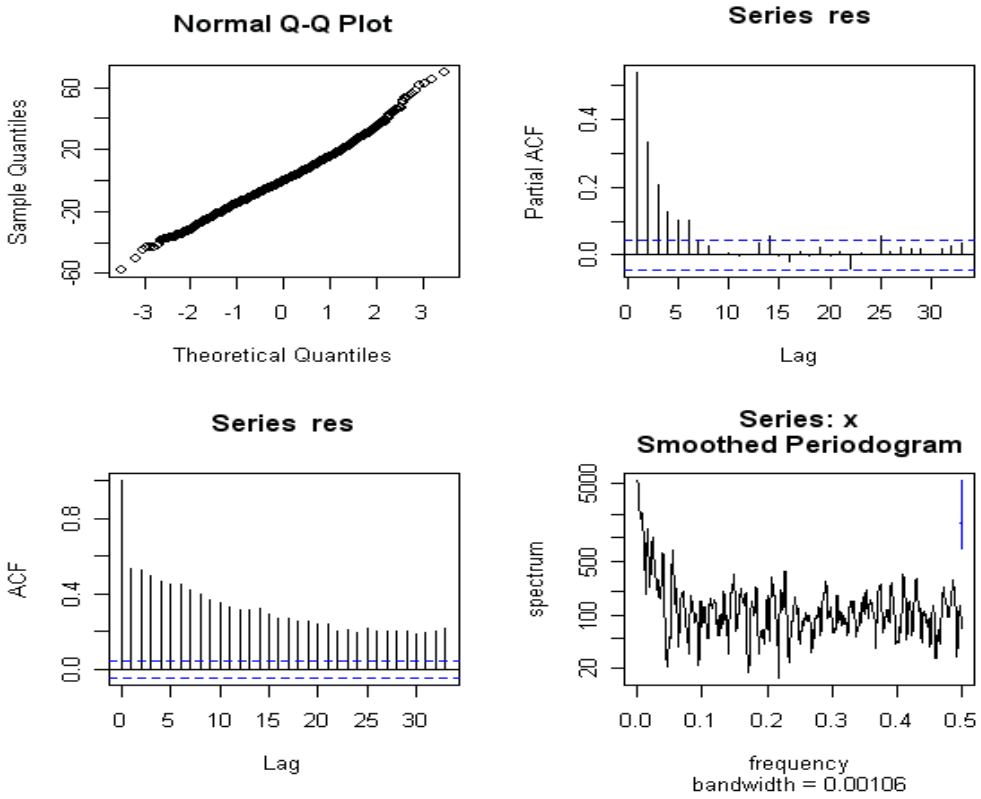

Figure 8.7 Analysis of residual from (16, 18). Normal Q-Q plot was very close to a straight line (top left panel). Partial autocorrelation function cut of at lag 6 (top right panel) and autocorrelation function tailed off (bottom left panel), therefore an AR(6) process. Smoothed periodogram of the residual were most in 95% confidence interval (bottom right panel).

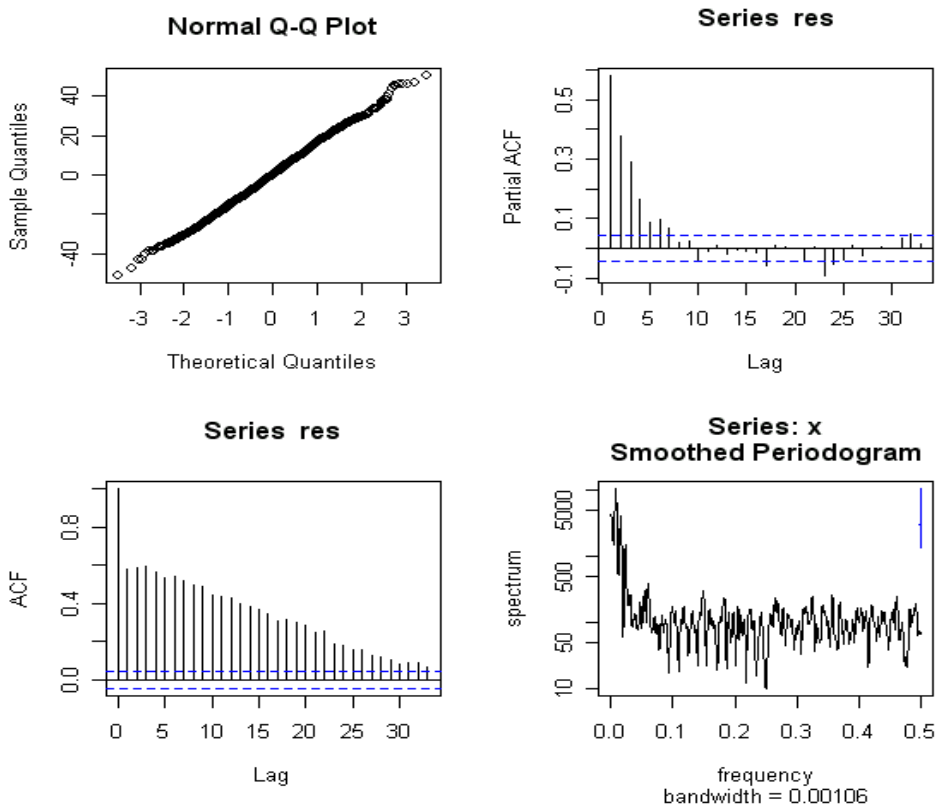

Figure 8.8 Analysis of residual from (29, 11). Normal Q-Q plot was very close to a straight line (top left panel). Partial autocorrelation function cut of at lag 7 (top right panel) and autocorrelation function tailed off (bottom left panel), therefore an AR(7) process. Smoothed periodogram of the residual were most in 95% confidence interval (bottom right panel).

8.4 Residual from complex demodulation was an AR process of order 6 to 7

AR models were fitted to the residuals according to PACF of the residuals. An AR(6) models was fitted to the residual after complex demodulated signal from (16,18) and AR(7) was fitted to the residual from (29, 11). The fitting of both models were diagnosed with the function tsdiag() in R and the results were shown in figure 8.9 and figure 8.10 respectively.

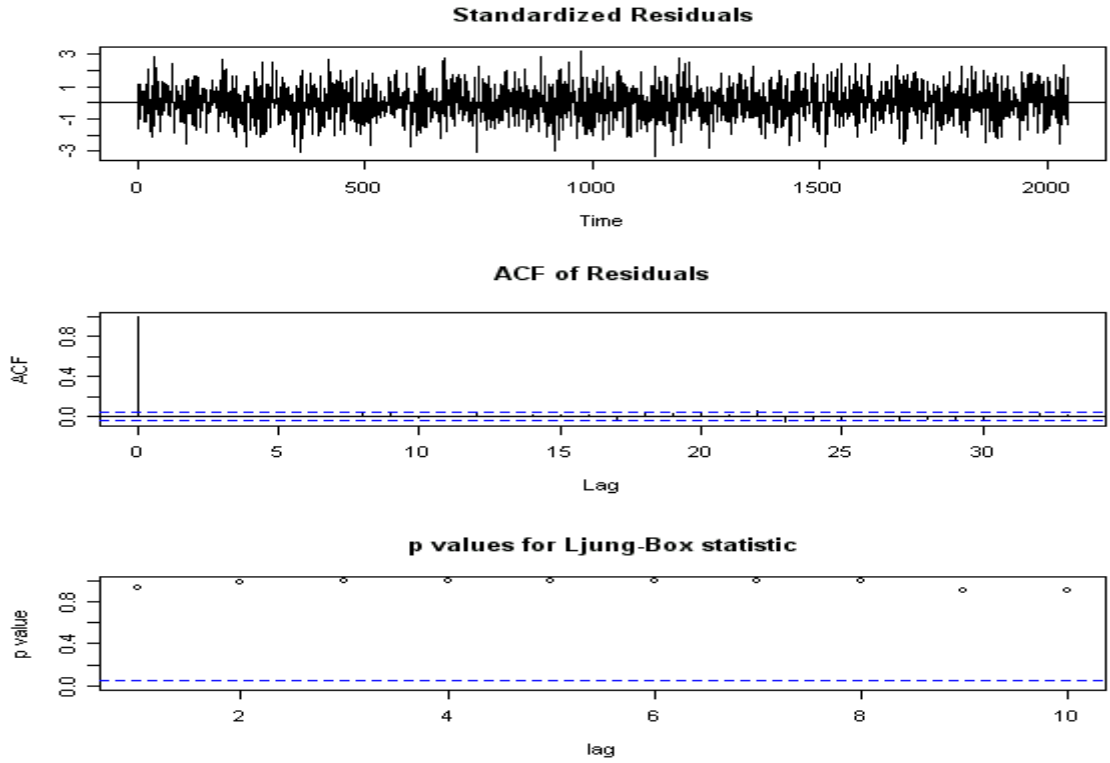

Figure 8.9 Fit an AR(6) model for the residual in figure 8.7

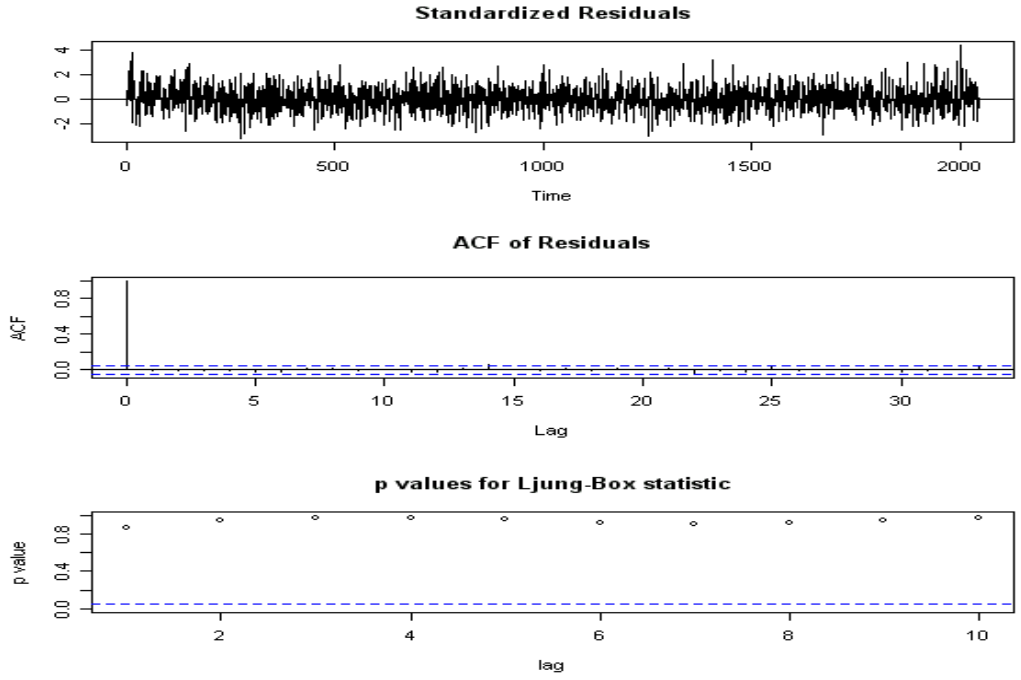

Figure 8.10 Fit an AR(7) model for the residual in figure 8.8

Besides the low frequency fluctuation as discussed in section 8.3, the standardized residual of the residuals appeared like white noise. ACF showed no correlation at any lags and the only value above the 95% confidence interval for 0 was at lag 0, therefore, the residual after fitting AR model did not depended on any previous or future values and verified that the thermo noise was an AR proecess. Ljung-Box statistics were used to tested the randomness and the blue dash lines gave the value correspond to $p=0.05$ and if $p<0.05$, it indicated not randome. The p-value of Ljung-Box statistics were well above 0.05 and the residuals were random. Therefore I concluded that complex demodulation was a right approach to analyze monomorphic VT. From the filtered signal, the isochronal map was obtained at each beat and the average of 30 beats shown in figure 8.11 illustrated the very similar damage pattern as that from CCF (figure 8.2).

8.5 Discussion

Theory of time series analysis was well established and widely applied in many fields. Given the complexity of optical mapping data, the approach provided a new way to analyze data efficiently. Both CCF approach in time domain and complex demodulation in frequency domain yielded satisfactory results in analyzing monomorphic VT. The method was also applied on periodical pacing data in chapter 7 and almost the same results were obtained with this approach as the traditional approach in chapter 7. The advantages of this approach include: 1) more data in MI could be included as it required less SNR than traditional approach; 2) more efficient as less signals needed manual correction. For example, ,the activation time, defined by largest dF/dt, would results in computed activation earlier than real activation in the second and last beats in figure 8.6

due to noise and this was corrected by either manual correction or left out signal from this point. Complex demodulation, in contrast, could automatically pick the activation time without sacrificing accuracy as noises were filter out. CCF avoided this kind of problem as CCF computed similarity not limited to one time spot but along the whole signal.

Despite the advantages of these two approaches, CCF could not be performed on polymorphic VT as dominant frequency changed along time and comparing the whole signal with more than one dominant frequencies could be misleading. Complex demodulation was a good way to go.

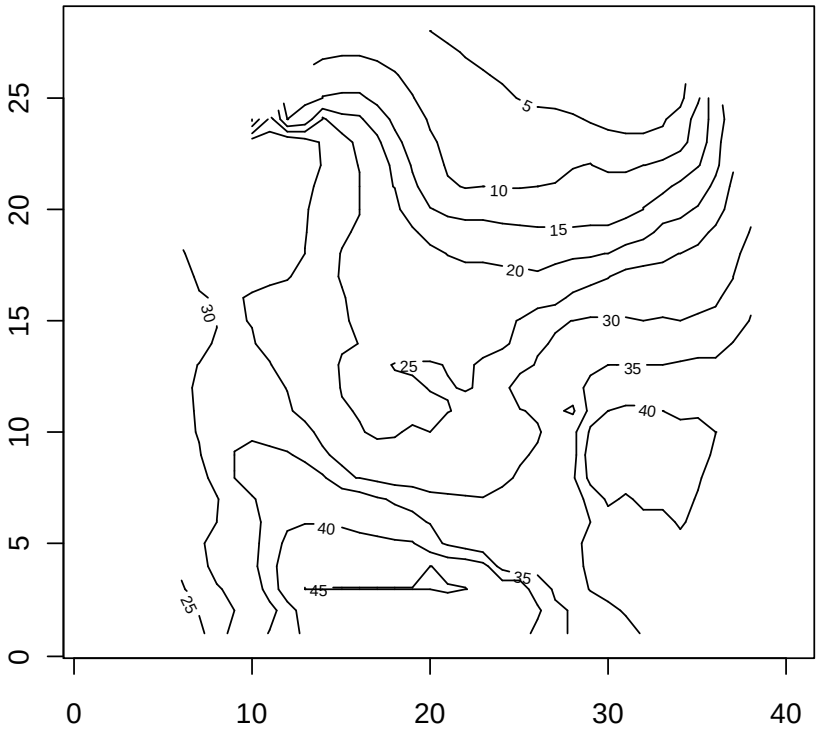

Figure 8.11 Isochronal map constructed from complex demodulation

Chapter 9:

Conclusion

Stem cell therapy for cardiac repair has blossomed in the past 10 years and continues to attract more interests from researchers to clinician. The plasticity of stem cells ignites the possibility of regenerates the heart, the last organ to be regenerated in body. The stem cell therapy was limited by the delivery methods due to the dilemma of non-invasiveness and delivery efficiency.

This thesis summarized the efforts from our group to a non-invasive and efficient BiAb targeting method to delivery stem cells to the damaged myocardium. BiAb production, characterization and titration were described in chapter 3. The ability of BiAb to deliver stem cells effectively in MI was verified in chapter 4. BiAb targeted HSCs not only more efficiently repaired the heart than the intravenously administrated unarmed HSCs (chapter 5) but also yielded at least comparable if not better improvement to direct injection unarmed HSCs into MI (chapter 6, 7). As more than half of patients with MI died directly from sudden arrhythmias, it is important to determine whether or not a stem cell therapy is proarrhythmia. Chapter 7 explored the electrophysiological effects of HSCs in treating MI and proved that HSCs are not proarrythymia and moreover BiAb targeted HSCs showed a trend of better electrophysiological properties maybe because the uniform repair nature for BiAb targeting. Chapter 8 attempted to introduce a new statistical method to process to large amount of electrophysiological data.

More questions need to be addressed like the clear mechanism of HSCs repairing the hearts; powerful proof of BiAb targeting is better than other methods by increasing the animal numbers in each group. However, we comfortably to conclude that BiAb targeted stem cells are beneficial and clinically relevant for treating MI.

Reference:

1. Lenfant, C., *Fixing the failing heart.* Circulation, 1997. **95**(4): p. 771-2.
2. Cohn, J.N., et al., *Report of the National Heart, Lung, and Blood Institute Special Emphasis Panel on Heart Failure Research.* Circulation, 1997. **95**(4): p. 766-70.
3. Thygesen, K., et al., *Universal definition of myocardial infarction.* Circulation, 2007. **116**(22): p. 2634-53.
4. el Oakley, R.M., et al., *Extended criteria for cardiac allograft donors: a consensus study.* J Heart Lung Transplant, 1996. **15**(3): p. 255-9.
5. Keck, B.M., et al., *Worldwide thoracic organ transplantation: a report from the UNOS/ISHLT International Registry for Thoracic Organ Transplantation.* Clin Transpl, 1999: p. 35-49.
6. Rubin, E.F., *Essential Patholgoy*. 2 ed. 1995, Philadelphia, PA: JB Lippincott Co.
7. Cotran, R.K. and S. Robbins, *Robbins Pathologic Basis of Disease* 5ed. 1994, Philadelphia, PA: WB Saunders Co.
8. Bajzer, C., *Acute Myocardial Infarction*. Cleveland Clinic MedicineIndex. 2002.
9. Swynghedauw, B., *Molecular mechanisms of myocardial remodeling.* Physiol Rev, 1999. **79**(1): p. 215-62.
10. Virag, J.I. and C.E. Murry, *Myofibroblast and endothelial cell proliferation during murine myocardial infarct repair.* Am J Pathol, 2003. **163**(6): p. 2433-40.
11. Braunwald, E. and M.R. Bristow, *Congestive heart failure: fifty years of progress.* Circulation, 2000. **102**(20 Suppl 4): p. IV14-23.
12. Swedberg, K., et al., *Guidelines for the diagnosis and treatment of chronic heart failure: executive summary (update 2005): The Task Force for the Diagnosis and Treatment of Chronic Heart Failure of the European Society of Cardiology.* Eur Heart J, 2005. **26**(11): p. 1115-40.
13. Casterella, P.J. and J.E. Tcheng, *Review of the 2005 American College of Cardiology, American Heart Association, and Society for Cardiovascular Interventions guidelines for adjunctive pharmacologic therapy during percutaneous coronary interventions: practical implications, new clinical data, and recommended guideline revisions.* Am Heart J, 2008. **155**(5): p. 781-90.
14. Jones, R.H., *The year in cardiovascular surgery.* J Am Coll Cardiol, 2008. **51**(17): p. 1707-18.
15. Condorelli, G., et al., *Cardiomyocytes induce endothelial cells to trans-differentiate into cardiac muscle: implications for myocardium regeneration.* Proc Natl Acad Sci U S A, 2001. **98**(19): p. 10733-8.
16. Menasche, P., et al., *Myoblast transplantation for heart failure.* Lancet, 2001. **357**(9252): p. 279-80.
17. Jackson, K.A., et al., *Regeneration of ischemic cardiac muscle and vascular endothelium by adult stem cells.* J Clin Invest, 2001. **107**(11): p. 1395-402.
18. Min, J.Y., et al., *Transplantation of embryonic stem cells improves cardiac function in postinfarcted rats.* J Appl Physiol, 2002. **92**(1): p. 288-96.

19. Reinecke, H., et al., *Survival, integration, and differentiation of cardiomyocyte grafts: a study in normal and injured rat hearts.* Circulation, 1999. **100**(2): p. 193-202.
20. Klug, M.G., et al., *Genetically selected cardiomyocytes from differentiating embronic stem cells form stable intracardiac grafts.* J Clin Invest, 1996. **98**(1): p. 216-24.
21. Murry, C.E., M.L. Whitney, and H. Reinecke, *Muscle cell grafting for the treatment and prevention of heart failure.* J Card Fail, 2002. **8**(6 Suppl): p. S532-41.
22. Hagege, A.A., et al., *Skeletal myoblast transplantation in ischemic heart failure: long-term follow-up of the first phase I cohort of patients.* Circulation, 2006. **114**(1 Suppl): p. I108-13.
23. Dib, N., et al., *Safety and feasibility of autologous myoblast transplantation in patients with ischemic cardiomyopathy: four-year follow-up.* Circulation, 2005. **112**(12): p. 1748-55.
24. Itescu, S., M.D. Schuster, and A.A. Kocher, *New directions in strategies using cell therapy for heart disease.* J Mol Med, 2003. **81**(5): p. 288-96.
25. Orlic, D., et al., *Mobilized bone marrow cells repair the infarcted heart, improving function and survival.* Proc Natl Acad Sci U S A, 2001. **98**(18): p. 10344-9.
26. Orlic, D., et al., *Bone marrow cells regenerate infarcted myocardium.* Nature, 2001. **410**(6829): p. 701-5.
27. Yeh, E.T., et al., *Transdifferentiation of human peripheral blood CD34+-enriched cell population into cardiomyocytes, endothelial cells, and smooth muscle cells in vivo.* Circulation, 2003. **108**(17): p. 2070-3.
28. Nygren, J.M., et al., *Bone marrow-derived hematopoietic cells generate cardiomyocytes at a low frequency through cell fusion, but not transdifferentiation.* Nat Med, 2004. **10**(5): p. 494-501.
29. Balsam, L.B., et al., *Haematopoietic stem cells adopt mature haematopoietic fates in ischaemic myocardium.* Nature, 2004. **428**(6983): p. 668-73.
30. Wagers, A.J., et al., *Little evidence for developmental plasticity of adult hematopoietic stem cells.* Science, 2002. **297**(5590): p. 2256-9.
31. Yang, J., et al., *Effects of Myocardial Transplantation of Marrow Mesenchymal Stem Cells Transfected with Vascular Endothelial Growth Factor for the Improvement of Heart Function and Angiogenesis after Myocardial Infarction.* Cardiology, 2006. **107**(1): p. 17-29.
32. Patel, A.N., et al., *Surgical treatment for congestive heart failure with autologous adult stem cell transplantation: a prospective randomized study.* J Thorac Cardiovasc Surg, 2005. **130**(6): p. 1631-8.
33. Archundia, A., et al., *Direct cardiac injection of G-CSF mobilized bone-marrow stem-cells improves ventricular function in old myocardial infarction.* Life Sci, 2005. **78**(3): p. 279-83.
34. Strauer, B.E., et al., *Repair of infarcted myocardium by autologous intracoronary mononuclear bone marrow cell transplantation in humans.* Circulation, 2002. **106**(15): p. 1913-8.

35. Sinha, S., et al., *Safety and efficacy of peripheral blood progenitor cell mobilization and collection in patients with advanced coronary heart disease.* J Clin Apher, 2006. **21**(2): p. 116-20.
36. Schachinger, V., et al., *Improved clinical outcome after intracoronary administration of bone-marrow-derived progenitor cells in acute myocardial infarction: final 1-year results of the REPAIR-AMI trial.* Eur Heart J, 2006. **27**(23): p. 2775-83.
37. *Baxter press release 2006; http://www.baxter.com/about_baxter/news_room/news_releases/2006/03-07-06-stem_cell_trial.html.*
38. Janssens, S., et al., *Autologous bone marrow-derived stem-cell transfer in patients with ST-segment elevation myocardial infarction: double-blind, randomised controlled trial.* Lancet, 2006. **367**(9505): p. 113-21.
39. Barbash, I.M. and J. Leor, *Myocardial regeneration by adult stem cells.* Isr Med Assoc J, 2006. **8**(4): p. 283-7.
40. Lum, L.G., et al., *Targeting of Lin-Sca+ hematopoietic stem cells with bispecific antibodies to injured myocardium.* Blood Cells Mol Dis, 2004. **32**(1): p. 82-7.
41. Lee, R.J., et al., *Antibody Targeting of Stem Cells to Infarcted Myocardium.* Stem Cells, 2006.
42. Lum, L.G., P.A. Davol, and R.J. Lee, *The new face of bispecific antibodies: targeting cancer and much more.* Exp Hematol, 2006. **34**(1): p. 1-6.
43. Zhao, T.C., et al., *Targeting human CD34+ hematopoietic stem cells with anti-CD45 x anti-myosin light-chain bispecific antibody preserves cardiac function in myocardial infarction.* J Appl Physiol, 2008. **104**(6): p. 1793-800.
44. Nugent, H.M. and E.R. Edelman, *Tissue engineering therapy for cardiovascular disease.* Circ Res, 2003. **92**(10): p. 1068-78.
45. Sievers, R.E., et al., *A model of acute regional myocardial ischemia and reperfusion in the rat.* Magn Reson Med, 1989. **10**(2): p. 172-81.
46. Springer, M.L., et al., *Closed-chest cell injections into mouse myocardium guided by high-resolution echocardiography.* Am J Physiol Heart Circ Physiol, 2005. **289**(3): p. H1307-14.
47. Litwin, S.E., et al., *Serial echocardiographic assessment of left ventricular geometry and function after large myocardial infarction in the rat.* Circulation, 1994. **89**(1): p. 345-54.
48. Ngan F Huang, R.E.S., Jennifer S Park, Qizhi Fang, Song Li & Randall J Lee, *A rodent model of myocardial infarction for testing the efficacy of cells and polymers for myocardial reconstruction.* Nature Protocols, 2006. **1**(3): p. 1596-1609.
49. Christman, K.L., et al., *Fibrin glue alone and skeletal myoblasts in a fibrin scaffold preserve cardiac function after myocardial infarction.* Tissue Eng, 2004. **10**(3-4): p. 403-9.
50. Lum, L.G., et al., *Virtual reality of stem cell transplantation to repair injured myocardium.* J Cell Biochem, 2005. **95**(5): p. 869-74.
51. Lee, M.S., M. Lill, and R.R. Makkar, *Stem cell transplantation in myocardial infarction.* Rev Cardiovasc Med, 2004. **5**(2): p. 82-98.

52. Frank, J.A., et al., *Clinically applicable labeling of mammalian and stem cells by combining superparamagnetic iron oxides and transfection agents.* Radiology, 2003. **228**(2): p. 480-7.
53. Arbab, A.S., et al., *Intracytoplasmic tagging of cells with ferumoxides and transfection agent for cellular magnetic resonance imaging after cell transplantation: methods and techniques.* Transplantation, 2003. **76**(7): p. 1123-30.
54. Orlic, D., *Adult BM stem cells regenerate mouse myocardium.* Cytotherapy, 2002. **4**(6): p. 521-5.
55. Orlic, D., J.M. Hill, and A.E. Arai, *Stem cells for myocardial regeneration.* Circ Res, 2002. **91**(12): p. 1092-102.
56. Orlic, D., et al., *Transplanted adult bone marrow cells repair myocardial infarcts in mice.* Ann N Y Acad Sci, 2001. **938**: p. 221-9; discussion 229-30.
57. Orlic, D., et al., *Bone marrow stem cells regenerate infarcted myocardium.* Pediatr Transplant, 2003. **7 Suppl 3**: p. 86-8.
58. Murry, C.E., et al., *Haematopoietic stem cells do not transdifferentiate into cardiac myocytes in myocardial infarcts.* Nature, 2004. **428**(6983): p. 664-8.
59. Chiu, R.C., A. Zibaitis, and R.L. Kao, *Cellular cardiomyoplasty: myocardial regeneration with satellite cell implantation.* Ann Thorac Surg, 1995. **60**(1): p. 12-8.
60. Zohlnhofer, D., et al., *Stem cell mobilization by granulocyte colony-stimulating factor for myocardial recovery after acute myocardial infarction: a meta-analysis.* J Am Coll Cardiol, 2008. **51**(15): p. 1429-37.
61. Dawn, B., et al., *Transplantation of bone marrow-derived very small embryonic-like stem cells attenuates left ventricular dysfunction and remodeling after myocardial infarction.* Stem Cells, 2008. **26**(6): p. 1646-55.
62. Engelmann, M.G., et al., *Autologous bone marrow stem cell mobilization induced by granulocyte colony-stimulating factor after subacute ST-segment elevation myocardial infarction undergoing late revascularization: final results from the G-CSF-STEMI (Granulocyte Colony-Stimulating Factor ST-Segment Elevation Myocardial Infarction) trial.* J Am Coll Cardiol, 2006. **48**(8): p. 1712-21.
63. Vanderheyden, M., et al., *Time-dependent effects on coronary remodeling and epicardial conductance after intracoronary injection of enriched hematopoietic bone marrow stem cells in patients with previous myocardial infarction.* Cell Transplant, 2007. **16**(9): p. 919-25.
64. Henning, R.J., et al., *Human cord blood cells and myocardial infarction: effect of dose and route of administration on infarct size.* Cell Transplant, 2007. **16**(9): p. 907-17.
65. Haider, H.K., L. Ye, and M. Ashraf, *Skeletal muscle derived stem cells for myocardial repair.* Recent Patents Cardiovasc Drug Discov, 2007. **2**(3): p. 205-13.
66. Bayly, P.V., et al., *Estimation of conduction velocity vector fields from epicardial mapping data.* IEEE Trans Biomed Eng, 1998. **45**(5): p. 563-71.
67. Verheule, S., et al., *Direction-dependent conduction abnormalities in a canine model of atrial fibrillation due to chronic atrial dilatation.* Am J Physiol Heart Circ Physiol, 2004. **287**(2): p. H634-44.

68. Everett, T.H.t., et al., *Left atrial dilatation resulting from chronic mitral regurgitation decreases spatiotemporal organization of atrial fibrillation in left atrium.* Am J Physiol Heart Circ Physiol, 2004. **286**(6): p. H2452-60.
69. Joung, B., et al., *Bone marrow mononuclear stem cells transplanted in rat infarct myocardium improved the electrical conduction without evidence of proarrhythmic effects.* Yonsei Med J, 2007. **48**(5): p. 754-64.
70. Shumway, R.H. and D.S. Stoffer, *Time Series Analysis and Its Applications with R Examples*. 2006, New York, NY: Springer.
71. Bolt, B.A. and D.R. Brillinger, *Estimation of uncertainties in eigenspectral estimates from decaying geophysical time series.* Geophys, J. R. astr. Soc., 1979. **59**: p. 593-603.

Publishing Agreement

It is the policy of the University to encourage the distribution of all theses and dissertations. Copies of all UCSF theses and dissertations will be routed to the library via the Graduate Division. The library will make all theses and dissertations accessible to the public and will preserve these to the best of their abilities, in perpetuity.

Please sign the following statement:

I hereby grant permission to the Graduate Division of the University of California, San Francisco to release copies of my thesis or dissertation to the Campus Library to provide access and preservation, in whole or in part, in perpetuity.

Yiping Gu 12/4/2008

Author Signature Date